TECHNICAL NOTES

NATIONAL ADVISORY COMMITTEE FOR AERONAUTICS

No. 626

STATIC THRUST ANALYSIS OF THE LIFTING AIRSCREW

By Montgomery Knight and Ralph A. Hefner
Georgia School of Technology

Washington
December 1937

NATIONAL ADVISORY COMMITTEE FOR AERONAUTICS

————————

TECHNICAL NOTE NO. 626

————————

STATIC THRUST ANALYSIS OF THE LIFTING AIRSCREW

By Montgomery Knight and Ralph A. Hefner

SUMMARY

This report presents the results of a combined theo-
retical and experimental investigation conducted at the
Georgia School of Technology on the static thrust of the
lifting airscrew of the type used in modern autogiros and
helicopters.

The theoretical part of this study is based on
Glauert's analysis but certain modifications are made that
further clarify and simplify the problem. Of these changes
the elimination of the solidity as an independent parameter
is the most important.

The experimental data were obtained from tests on four
rotor models of two, three, four, and five blades and, in
general, agree quite well with the theoretical calcula-
tions.

The theory indicates a method of evaluating scale ef-
fects on lifting airscrews, and these corrections have
been applied to the model results to derive general full-
scale static thrust, torque, and figure-of-merit curves
for constant-chord, constant-incidence rotors.

Convenient charts are included that enable hovering-
flight performance to be calculated rapidly.

INTRODUCTION

The problem of greater safety in flight is today com-
manding more and more attention. Two different methods of
attack are being developed at present. One of these con-
sists of improving the conventional fixed-wing airplane
through such modifications as Handley Page slots, wing
profiles giving smooth maximum lift characteristics, meth-
ods of obtaining more complete rolling and yawing control

in stalled flight, and other special devices. The alterna-
tive method is that of developing a type of aircraft in
which there will always be relative motion between the lift-
ing surfaces and the air, regardless of the motion or atti-
tude of the aircraft as a whole. This type is exemplified
by the autogiro and the various experimental helicopters,
of which the Bréguet-Dorand is the most outstanding recent
example (reference 1).

In order to investigate the possibilities of the
rotating-wing type of aircraft, a general study of the ver-
tical motion of the lifting airscrew has been undertaken
at the Daniel Guggenheim School of Aeronautics of the
Georgia School of Technology. This project is receiving
financial support from the National Advisory Committee for
Aeronautics and the State Engineering Experiment Station
of Georgia.

The purpose of this report is to present the results
of the first part of this investigation, which covers the
phase of static thrust or hovering flight of the helicop-
ter. Glauert's assumptions (reference 2) furnish the
background for the theoretical portion of the study. How-
ever, the induced velocity through the rotor is determined
on the basis of vortex theory rather than by using the con-
cept of the "actuator disk." This change has been made
because the vortex theory offers a much clearer picture of
the mechanism of airscrew thrust without materially com-
plicating the derivation of the induced velocity equation
which is identical for both methods.

The experimental part of the analysis provides numer-
ical values of such parameters as are essentially empirical
and serves to show the agreement between the calculated and
actual values of thrust and torque for four different ro-
tor models.

STATIC THRUST ANALYSIS

Basic assumptions.- In treating the complex problem
of the lifting airscrew, it is necessary to make the fol-
lowing simplifying assumptions:

1. The number of blades may be taken as infinite.

2. Induced angles of attack are sufficiently small
       so that the angle may be substituted for the
       sine and tangent, and the cosine replaced by
       unity.

3. Rotational and radial components of velocity and
tip effects may be neglected.

4. The slipstream contraction may be neglected.

Induced velocity.- The first step in the static thrust
analysis is to determine the downward velocity induced by
the motion of the blades. In the simplest case, each blade
of the rotor may be replaced by a rotating lifting line from
the ends of which spring trailing vortices. The tip vortex
will obviously form a helix in space while the vortex ema-
nating from the blade root will be concentric with the axis
of rotation, and in the present discussion its effect will
be neglected.

Since we are assuming an infinite number of blades the
problem consists of determining the velocity induced nor-
mal to the plane of the rotor by a cylindrical surface of
vorticity, bounded on one end by the rotor and extending
downward to infinity. Figure 1 depicts this cylinder with
its top in the xy plane and its axis coincident with the
−z axis. The ring s of width dz is an element of this
surface normal to the axis.

If we take the total circulation produced by the rotor
blades as Γ, the circulation strength of the ring s
will be $\dfrac{d\Gamma}{dz}\, dz$, and by neglecting higher order terms the
ring becomes equivalent to a circular vortex element of
radius R. It will be noted that $\dfrac{d\Gamma}{dz}$ = constant.

Now the potential at a point P due to a closed vor-
tex element may be expressed in the following form (refer-
ence 3):

$$\Phi_P = \frac{\Gamma'}{4\pi}\, \omega$$

where Γ' is the circulation about the element

and ω is the solid angle at P subtended by the
element

Thus, if the point P be in the plane of the rotor,
as shown in figure 1, we may write:

$$d\Phi_P = \frac{\dfrac{d\Gamma}{dz}\, dz}{4\pi}\, \omega$$

where ω is the solid angle at P subtended by the vortex ring s. The total potential at P will then be

$$\Phi_P = -\frac{\frac{d\Gamma}{dz}}{4\pi} \int_{Z_1}^{Z_2} \omega \, dz \tag{1}$$

The velocity at P, due to s, normal to the rotor plane, may now be obtained by differentiating with respect to z:

$$w_P = \frac{d\Phi}{dz} = -\frac{\frac{d\Gamma}{dz}}{4\pi} \left[\omega(Z_2) - \omega(Z_1) \right]$$

and for the entire cylinder where $Z_2' = -\infty$ and $Z_1 = 0$:

$$\omega(Z_2) = 0 \quad \text{and} \quad \omega(Z_1) = 2\pi$$

$$\therefore \, w_p = -\frac{1}{2} \frac{d\Gamma}{dz} = \text{constant} \tag{2}$$

It is important to note also that at the point p' in the plane of the rotor but beyond the blade tips, $\omega(Z_2) = \omega(Z_1) = 0$ and

$$\therefore \, w_{p'} = 0 \tag{3}$$

Thus we have established the fact that the vertical component of induced velocity is constant over the rotor disk since $\Gamma = \text{constant}$. Moreover, outside the disk this component is zero. It should also be observed that, if the point P is moved downward inside the vortex cylinder to a great distance from the rotor disk, the solid angle subtending it will become 4π, since the cylinder may then be considered doubly infinite in extent. Consequently,

$$\therefore \, w_p = -\frac{d\Gamma}{dz} \tag{4}$$

thus corroborating the well-known fact that the slipstream velocity in the plane of an airscrew is half that at a large distance downstream.

To investigate the general case of the induced velocity due to any distribution whatsoever of the circulation along the blade, we may proceed as follows. Consider a

blade element of length dr at a distance r from the
axis, as shown in figure 2. Let the circulation at r be
Γ. The circulation at r + dr will then be $(\Gamma + \frac{d\Gamma}{dr} dr)$.

According to equation (3) the induced velocities <u>out-
side</u> the respective cylindrical surfaces will be zero,
whereas <u>inside</u> they will be

$$w = -\frac{1}{2} \frac{d(\Gamma + \frac{d\Gamma}{dr} dr)}{dz} = -\frac{1}{2} \frac{d\Gamma}{dz} \quad \text{from} \quad r \quad \text{to} \quad r + dr$$

and

$$w = \frac{1}{2}\left[\frac{d\Gamma}{dz} - \frac{d(\Gamma + \frac{d\Gamma}{dr} dr)}{dz}\right] = 0 \quad \text{from} \quad 0 \quad \text{to} \quad r$$

these results being obtained by neglecting the higher order
infinitesimals.

This simple demonstration verifies the independence
of airscrew blade elements, which is a customary assumption
in modern airscrew analysis.

Having obtained the induced-velocity relationships due
to the vortex field, we will now derive a general expres-
sion for the circulation Γ as a function of the blade-
profile characteristics. Consider an element of a blade of
length dr at a distance r from the axis of rotation.
The thrust on this element will be

$$dT = \rho \frac{\Gamma}{B} \Omega r \, dr = \frac{\rho}{2} C_L \Omega^2 r^2 c \, dr \tag{5}$$

where   B is the number of blades

c, blade chord

Ω, angular velocity

Making the customary assumption that C_L varies linearly
with angle of attack α, we may write with the aid of fig-
ure 3:

$$C_L = a_0 \alpha$$
$$= a_0 (\theta - \varphi)$$

where a_0 is the lift curve slope for two-dimensional flow

    θ, blade incidence angle

    φ, $\tan^{-1} \dfrac{w}{\Omega r} = \dfrac{w}{\Omega r}$ = induced angle of flow

From equation (5) we may now write the circulation as

$$\Gamma = \frac{B}{2} \frac{c}{} a_0 (\theta - \varphi) \Omega r \qquad\qquad (6)$$

The distance between successive turns of the vortical helix is

$$d = \frac{2\pi r}{B} \sin \varphi$$

$$= \frac{2\pi r}{B} \frac{w}{\Omega r}$$

$$= \frac{2\pi w}{\Omega B}$$

and since

$$\frac{d\Gamma}{dz} = \frac{\Gamma}{Bd} = 2w$$

we obtain from (6) that

$$2w = \frac{\dfrac{a_0 c}{2} (\theta - \varphi) \Omega r}{\dfrac{2\pi w}{\Omega B}}$$

or

$$w^2 = \frac{a_0}{8} \frac{Bc}{\pi} (\theta - \varphi) \Omega^2 r \qquad\qquad (7)$$

In this analysis we shall confine ourselves to the case of blades of constant chord and hence the rotor solidity, as usually expressed, is

$$\sigma = \frac{Bc}{\pi} \frac{R}{R^2} = \frac{Bc}{\pi R}$$

Putting $x = \dfrac{r}{R}$

equation (7) becomes:

$$\left(\frac{w}{\Omega Rx}\right)^2 = \frac{\sigma a_0}{8x} (\theta - \varphi) = \varphi^2 \tag{7a}$$

or

$$\varphi^2 + \frac{\sigma a_0}{8x} \varphi - \frac{\sigma a_0}{8x} \theta = 0$$

The useful root of this quadratic is

$$\varphi = \frac{1}{2} \left[- \frac{\sigma a_0}{8x} + \sqrt{\left(\frac{\sigma a_0}{8x}\right)^2 + 4 \left(\frac{\sigma a_0}{8x}\right) \theta} \right]$$

Dividing both sides by σ we obtain:

$$\frac{\varphi}{\sigma} = \frac{1}{2x} \left[\sqrt{\left(\frac{a_0}{8}\right)^2 + 4 \left(\frac{a_0}{8}\right) \frac{\theta x}{\sigma}} - \frac{a_0}{8} \right]$$

and putting $\varphi_\sigma = \dfrac{\varphi}{\sigma}$

$$\theta_\sigma = \frac{\theta}{\sigma}$$

we have

$$\varphi_\sigma = \frac{1}{2x} \left[\sqrt{\left(\frac{a_0}{8}\right)^2 + 4 \left(\frac{a_0}{8}\right) \theta_\sigma x} - \frac{a_0}{8} \right] \tag{8}$$

which is identical with the result obtainable by the use of the momentum equation, i.e., the "actuator disk" method.

It should be noted that equation (8) is a general expression for the induced flow angle in terms of the radius variable x and the two parameters θ_σ and a_0. However, a_0 is substantially constant, varying but slightly with profile thickness and Reynolds Number. Thus, equation (8) effectively gives φ_σ as a function of the single parameter θ_σ, which results in a marked simplification of the analysis as originally presented by Glauert (reference 2).

In the first part of the previous analysis each blade

was replaced by a lifting line, i.e., Γ = constant. Therefore, equation (6) may be written:

$$\Gamma = \frac{Bc}{2} a_0 \, (\theta - \varphi) \, \Omega r = \frac{Bc}{2} a_0 \, (\theta_0 - \varphi_0) \, \Omega R$$

or $\qquad\qquad (\theta - \varphi) \, r = (\theta_0 - \varphi_0) \, R$

where θ_0 and φ_0 refer to the tip of the blade, but since $\varphi = w/\Omega r$

$$\left(\theta - \frac{w}{\Omega r} \right) = \left(\theta_0 - \frac{w}{\Omega R} \right) \frac{R}{r}$$

$$\therefore \quad \theta = \frac{\theta_0}{x} \qquad\qquad (9)$$

This is the variation in θ along the blade that is required to give constant circulation and uniform induced velocity. Over the effective portion of the blade

$$x > \frac{1}{4}, \quad \theta = \frac{\theta_0}{x} = \tan^{-1} \frac{\theta_0}{x} \quad (\text{approx.})$$

which defines the screw surface described by each blade, if it were moving in a solid medium. Therefore, equation (9) may be considered to represent the "constant pitch" airscrew, and the induced angle function becomes

$$\varphi_{\sigma_0} = \varphi_\sigma \, x = \frac{1}{2} \left[\sqrt{\left(\frac{a_0}{8} \right)^2 + 4 \left(\frac{a_0}{8} \right) \theta_{\sigma_0}} - \frac{a_0}{8} \right] \qquad (10)$$

For the type of rotor with untwisted blades, i.e., constant incidence

$$\varphi_\sigma = \frac{1}{2x} \left[\sqrt{\left(\frac{a_0}{8} \right)^2 + 4 \left(\frac{a_0}{8} \right) \theta_\sigma \, x} - \frac{a_0}{8} \right] \qquad (11)$$

where $\qquad\qquad\qquad \theta_\sigma$ = constant

Thrust.- The thrust produced by the rotor may be expressed as follows:

$$T = \frac{\rho}{2} \pi R^2 \, \Omega^2 \, R^2 \, C_T$$

where C_T is the nondimensional thrust coefficient.

To determine the thrust in terms of the rotor parameters, we write:

$$T = \frac{\rho}{2} Bc \int_0^R C_L \Omega^2 r^2 \, dr$$

$$= \frac{\rho}{2} Bc R^3 a_0 \int_0^1 (\theta - \varphi) \Omega^2 x^2 \, dx$$

or

$$C_T = \sigma a_0 \int_0^1 (\theta - \varphi) x^2 \, dx$$

and dividing by σ^2

$$\frac{C_T}{\sigma^2} = a_0 \int_0^1 (\theta_\sigma - \varphi_\sigma) x^2 \, dx \qquad (12)$$

This new thrust coefficient will be designated as

$$T_\sigma = \frac{C_T}{\sigma^2}$$

For the constant pitch rotor

$$T_\sigma = a_0 \int_0^1 \left(\frac{\theta_{\sigma_0}}{x} - \varphi_\sigma \right) x^2 \, dx$$

$$= \frac{a_0}{2} (\theta_{\sigma_0} - \varphi_{\sigma_0}) \qquad (13)$$

where $\varphi_{\sigma_0} = \frac{1}{2} \left[\sqrt{\left(\frac{a_0}{8}\right)^2 + 4 \left(\frac{a_0}{8}\right) \theta_{\sigma_0}} - \frac{a_0}{8} \right]$

And for the constant-incidence rotor

$$T = a_0 \int_0^1 \left[\theta_\sigma - \frac{1}{2x} \left(\sqrt{\left(\frac{a_0}{8}\right)^2 + 4 \left(\frac{a_0}{8}\right) \theta_\sigma x} - \frac{a_0}{8} \right) \right] x^2 \, dx$$

and upon integrating

$$T_\sigma = a_0 \left\{ \frac{\theta_\sigma}{3} + \frac{1}{4}\left(\frac{a_0}{8}\right) - \frac{1}{16\,\theta_\sigma{}^2\left(\frac{a_0}{8}\right)^2}\left[\frac{A^5}{5} - \left(\frac{a_0}{8}\right)^2 \frac{A^3}{3} + \right.\right.$$

$$\left.\left. + \frac{2}{15}\left(\frac{a_0}{8}\right) \right] \right\} \qquad (14)$$

where $\qquad A = \sqrt{\left(\frac{a_0}{8}\right)^2 + 4\left(\frac{a_0}{8}\right)\theta_\sigma}$

Torque.— The rotor torque may be written as

$$Q = \frac{\rho}{2}\,\pi\,R^2\,\Omega^2\,R^3\,C_Q$$

C_Q = nondimensional torque coefficient

The torque may be divided into three parts analogous to the partition of drag on an airfoil. These are:

       1. Induced torque.

       2. Minimum profile torque.

       3. Profile variation torque.

The induced torque due to the inclination of the air-foil lift vector, figure 3, is

$$Q_i = \frac{\rho}{2}\,Bc \int_0^R C_L \sin\varphi\,\Omega^2\,r^3\,dr$$

$$= \frac{\rho}{2}\,Bc\,R^4\,a_0 \int_0^1 \varphi\,(\theta - \varphi)\,\Omega^2\,x^3\,dx \quad (\text{approx.})$$

or $\qquad C_{Q_i} = \sigma\,a_0 \int_0^1 \varphi\,(\theta - \varphi)\,x^3\,dx$

The minimum profile torque is

$$Q_\delta = \frac{\rho}{2} Bc \int_0^R \delta \, \Omega^2 \, r^3 \, dr$$

$$= \frac{\rho}{2} Bc \, R^4 \, \delta \int_0^1 \Omega^2 \, x^3 \, dx$$

or

$$C_{Q_\delta} = \sigma \, \delta \int_0^1 x^3 \, dx$$

where

$$\delta = C_{D_{o_{min}}}$$

Assuming that the profile drag variation may be expressed as

$$\Delta \, C_{D_o} = \epsilon \, \alpha^2$$

where ϵ = const.

The profile variation torque may be written as

$$Q_\sigma = \frac{\rho}{2} Bc \int_0^R \epsilon \, \alpha^2 \, \Omega^2 \, r^3 \, dr$$

$$= \frac{\rho}{2} Bc \, R^4 \, \epsilon \int_0^1 (\theta - \varphi)^2 \, \Omega^2 \, x^3 \, dx$$

or

$$C_{Q_o} = \sigma \, \epsilon \int_0^1 (\theta - \varphi)^2 \, x^3 \, dx$$

For the constant pitch rotor the total torque coefficient may be expressed in the new form to eliminate σ as an independent parameter as follows:

$$Q_\sigma = \frac{C_Q}{\sigma^3} \quad \frac{\delta}{\sigma^2} \int_0^1 x^3 \, dx + \epsilon \int_0^1 \left(\frac{\theta \sigma_o}{x} - \varphi_\sigma \right)^2 x^3 \, dx +$$

$$+ a_o \int_0^1 \varphi_\sigma \left(\frac{\theta \sigma_o}{x} - \varphi_\sigma \right) x^3 \, dx \qquad (15)$$

But since

$$\varphi_\sigma \; x = \frac{w}{\Omega \; Rx} \; x = \varphi_{\sigma_0} = \frac{r}{2} \left(\sqrt{\left(\frac{a_0}{8}\right)^2 + 4 \left(\frac{a_0}{8}\right) \theta_{\sigma_0}} - \frac{a_0}{8} \right)$$

$$Q_\sigma = \frac{\delta}{4 \sigma^2} + \frac{\epsilon}{2} \left(\theta_{\sigma_0} - \varphi_{\sigma_0} \right)^2 + \frac{a_0}{2} \varphi_{\sigma_0} \left(\theta_{\sigma_0} - \varphi_{\sigma_0} \right) \quad (16)$$

In like manner the torque coefficient may be obtained for the constant incidence rotor as

$$Q_\sigma = \frac{\delta}{4\sigma^2}$$

$$+ \frac{\epsilon}{2} \left\{ \frac{\theta^2}{2} + \frac{4}{3} \left(\frac{a_0}{8}\right) - \frac{1}{2} \left(\frac{a_0}{8}\right)^2 \frac{1}{16 \; \theta_\sigma^2 \left(\frac{a_0}{8}\right)^3} \right.$$

$$\left. \left[\frac{A^7}{7} - \left(\frac{a_0}{8}\right)^4 \frac{A^3}{3} + \frac{4}{21} \left(\frac{a_0}{8}\right)^7 \right] \right\} -$$

$$- \left\{ 4\theta_\sigma \left(\frac{a_0}{8}\right)^2 + 2 \left(\frac{a_0}{8}\right)^3 - \frac{8}{\theta_\sigma^2 \left(\frac{a_0}{8}\right)^2} \left[\frac{A^7}{7} + 2 \left(\frac{a_0}{8}\right)^2 \frac{A^5}{5} - \right. \right.$$

$$\left. \left. - \left(\frac{a_0}{8}\right)^4 A^3 + \frac{48}{105} \left(\frac{a_0}{8}\right)^7 \right] \right\} \quad (17)$$

where, as in the thrust equation (14)

$$A = \sqrt{\left(\frac{a_0}{8}\right)^2 + 4 \left(\frac{a_0}{8}\right) \theta_\sigma}$$

Figure of merit.- Since for the condition of static thrust the rotor is not moving in translation, the ordinary concept of efficiency must be modified in order to devise a method of measuring the "lifting efficiency" of the helicopter airscrew. Glauert in reference 2 has designated this criterion as the "figure of merit" and has defined it as

$$M' = \frac{C_T^{3/2}}{C_Q}$$

This expression may be arrived at by noting that

$$\frac{T}{P} = \frac{C_T \; \Omega^2 \; R^2}{C_Q \; \Omega^3 \; R^3}$$

where P is the power applied to rotor; and to eliminate the tangential velocity ΩR, we may write:

$$\frac{T^{3/2}}{P} = \frac{C_T^{3/2}}{C_Q} = M'$$

and in terms of the new coefficients

$$M' = \frac{\left(\dfrac{C_T}{\sigma^2}\right)^{3/2}}{\left(\dfrac{C_Q}{\sigma^3}\right)} = \frac{T_\sigma^{3/2}}{Q_\sigma} \qquad (18)$$

The theoretical maximum or ideal value of M would occur if δ and ϵ were zero and its value may be obtained easily for the constant pitch rotor. Referring to (7a),

$$a_0 \left(\theta_{\sigma_0} - \varphi_{\sigma_0}\right) = 8 \, \varphi_{\sigma_0}^2$$

$$T_\sigma = \frac{a_0 \left(\theta_{\sigma_0} - \varphi_{\sigma_0}\right)}{2} = 4\varphi_{\sigma_0}^2$$

$$Q_{\sigma_i} = \frac{\varphi_{\sigma_0} \left(\theta_{\sigma_0} - \varphi_{\sigma_0}\right)}{2} = 4\varphi_{\sigma_0}^3$$

or $\qquad Q_{\sigma_i} = \dfrac{T_\sigma^{3/2}}{2}$

and hence $\qquad M'_I = 2$

The ideal figure of merit for the constant incidence rotor is not a constant and cannot be easily obtained as an analytical expression. However, the numerical values have been computed and these are given later.

The figure of merit may be defined on the basis of unity, as in the usual definition of efficiency by writing

$$M = \frac{1}{2} \frac{T_\sigma^{3/2}}{Q_\sigma}$$

and this form will be used in the subsequent discussion.

EXPERIMENTAL DATA

In order to obtain the values of the airfoil parameters appearing in the theory and to enable the calculated values of the rotor coefficients to be compared with tests on actual rotors, two sets of tests were made in the 9-foot wind tunnel of the Daniel Guggenheim School of Aeronautics.

Rotor model tests.- Four rotor models having two, three, four, and five blades and a diameter of 5 feet, were tested. Five blades and three hubs were used. The blades were identical and interchangeable, thus making possible the four rotor combinations.

The blades had the N.A.C.A. 0015 symmetrical profile (reference 4) and were of 2-inch chord from the tip to a radius of 5 inches. From this point they were faired into a 3/4-inch circle at a radius of 1.5 inches. The diameter of the hubs was 3 inches. Horizontal hinges were located in the hub at a radius of 1 inch to permit vertical articulation of the blades. A split sleeve with clamping screws at the inner end of each blade enabled the blade incidence to be changed. The blade plan form was straight and there was no twist.

In order to prevent any tendency to twist when in operation, the blades were statically balanced about the quarter-chord point by using a steel leading edge recessed into the laminated wood of the blade and the quarter-chord line was radial. The blade tip in cross section was semicircular.

The various rotors were mounted on the frame of the wind-tunnel balance as shown in figure 4. The rotor drive shaft was horizontal as shown, and was 12 inches long, terminating in a small gear box at the center of the tun-

nel jet. This gear box was held by a torque tube support-
ed on a tripod attached to the balance frame and extending
below the jet to a motor-driven worm and pinion, enabling
the angle of attack of the rotor to be varied through 360°.

Inside this torque tube was the main drive shaft which
was turned by a 1-horsepower 3-phase induction motor
through a V-belt drive. Since all this equipment was
mounted on the six-component balance frame, it constitued
a dynamometer capable of measuring the thrust and torque on
the rotor for any position of the model.

The six-component balance of this wind tunnel upon
which both the rotor and airfoil tests were made, is some-
what unusual in that it utilizes a hydraulic method of
transmitting the forces to a central point where they are
automatically balanced and indicated pneumatically. The
U frame which holds the model is held in place by six tubu-
lar struts, each of which terminates in a hydraulic cell.
These cells consist of a shallow cylinder containing a
loose-fitting piston. The 1/8-inch annular space between
the piston and cylinder is covered with 0.020-inch thick
pure gum rubber, thus providing a tight but substantially
frictionless seal. The cells are completely filled with
distilled water and the pressure due to the force applied
on each cell is transmitted through small copper tubing to
identical cells mounted on the frame shown in the right
background of figure 4. Here the forces are combined by a
rigid connection between the pistons of the appropriate
cells so as to give the total force. These forces are in
turn applied to the pistons of similar cells actuated by
air, and the pressures in these air cells are controlled
automatically by means of special piston-type valves which
apply either pressure or vacuum to the cells, depending
upon the direction of the forces. Since the pressure in
each air cell at any time is a measure of the particular
force applied to it, these cells are tapped and the pres-
sure transmitted through rubber tubing to a manifold which
is fitted with six valves. From this manifold another rub-
ber tube goes to an additional cell unit of the same type
mounted on the platform of a dial scale. Thus a single
operator may read all the forces in any desired sequence
by opening the appropriate manifold valves. The sensitiv-
ity of the balance can be changed by substituting balanc-
ing air cells of different sizes or by using water or al-
cohol manometers in place of the dial scale. Forces as
small as 1 gram or as large as 150 kilograms can be meas-
ured with the present arrangement. This range could easi-

ly be extended. The system is practically null in operation, since the maximum movement of the balance frame is never greater than about 1/64 inch.

The balance has proved quite satisfactory over a period of three years, the only attention necessary being an occasional replacement of the rubber portions of the diaphragms and cleaning of the piston valves. It has proved to be convenient and flexible in its operation, since it not only enables a single operator to make all ordinary tests but it is also possible to move the indicating mechanism wherever desired.

The average rotational speed of the model rotors was approximately 960 r.p.m. This varied slightly with the number of blades and with the incidence because of the induction motor slip and the creep of the belt drive under load, but not sufficiently to cause an appreciable change in Reynolds Number. The speed readings were obtained by means of an ordinary hand tachometer and stop watch, the average of three 30-second readings being used.

In order to obtain consistent and reliable thrust and torque readings, it was found that certain precautions had to be taken. It was necessary to set the blade-incidence angles within plus or minus 0.05°. This was finally accomplished with the aid of the apparatus shown in figure 5. The rotor hub was clamped rigidly to a horizontal support and the tip of each blade in turn was attached by a special clamping device to a sensitive inclinometer mounted on ball bearings and counterweighted so that it imposed no restraint on the flexible blade. The inclinometer was sensitive to within one minute of angle.

There was found to be a slight lack of uniformity in the blades due to warping. Since, for uniform results, it was necessary to set the blade angle with respect to the zero thrust angle, the thrust curves of each blade were obtained by running them singly with a balancing counterweight. Two of the blades showed no effective twist and the worst one had a twist of 40 minutes. In making the final tests these twist corrections were used in setting the blade angles.

Various positions of the model with respect to the tunnel were investigated and the final position chosen was that shown in figure 4 with the slipstream toward the left since in this position no interference effects were apparent.

The precision of the measurements was as follows:

Thrust . . . . ±1 percent

Torque . . . . ±1 percent

Minimum torque . . . ±2 percent

Rate of rotation . . ±½ percent

Blade incidence angle ±0.05°

Airfoil tests.- In the above mathematical analysis, the airfoil profile characteristics of the rotor blades were assumed to be as follows:

$$C_L = a_0 \, \alpha$$

$$C_{D_0} = C_{D_{0_{min}}} + \epsilon \, \alpha^2$$

where α is the effective angle of attack of the airfoil.

In order to obtain quantitative results from the theoretical equations of thrust and torque, it was necessary to determine specific values of a_0 and $C_{D_{0_{min}}}$, both of which are functions of the Reynolds Number. This was done by testing an airfoil of N.A.C.A. 0015 profile in the wind tunnel at approximately the same Reynolds Number (242,000) as that of the rotor-blade tips. This airfoil had a span of 6 feet and a chord of 6 inches and was mounted in the wind tunnel as shown in figure 6, which is a view of the set-up looking in the upstream direction.

The model was supported on a streamlined fork located at the midspan and quarter-chord point and on a small oval rod which was connected to a short sting attached to the trailing edge. This latter rod was actuated by a push-pull rod sliding inside the torque tube which held the fork and was attached to the balance frame. The push rod was actuated by a second motor-driven worm and pinion mechanism permitting remote control of the angle of attack. The angle readings were effected by means of a simple direct-current bridge system with the galvanometer and the adjustable leg of the bridge mounted on the balance-control table.

The balance frame and the model-supporting tripod were shielded as shown to reduce the tare forces. These tare forces were measured with the model supported at the tips and with the fork and incidence rod in place but not touching the airfoil and were found to be zero for the lift and about 60 percent of the minimum profile drag.

The air flow in the jet is reasonably smooth and uniform owing to the 5 to 1 contraction in the collector. The variation of dynamic pressure over the span of the model is within plus or minus 1 percent. As previously mentioned, the jet is 9 feet in diameter and 12 feet long, and the model is located with its quarter-chord point on the lateral axis of the balance, which is 3 feet downstream from the entrance cone.

In these tests the dynamic pressure was held constant by means of an alcohol manometer connected to four static plates located in the large section of the entrance cone, the static plate pressure having been previously calibrated against pitot surveys made in the model position.

The precision of measurements in the airfoil tests was as follows:

Lift . . . . ± 1 percent

Drag . . . . . ± 1 percent

Minimum drag . . ± 2 percent

Velocity . . . . . $\pm \frac{1}{2}$ percent

Angle of attack $\pm 0.05°$

Reduction of data.- The formulas used for reducing the thrust and torque measurements from the four rotor tests are as follows:

$$C_T = \frac{2T}{\rho \pi R^2 \Omega^2 R^2}$$

$$T_\sigma = \frac{C_T}{\sigma^2}$$

$$C_Q' = \left(\frac{2Q}{\rho \pi R^2 \Omega^2 R^3} - \frac{8\sigma}{4} \right)$$

$$Q_\sigma' = \left(\frac{C_Q}{\sigma^3} - \frac{8}{4\sigma^2} \right)$$

The thrust and torque coefficients C_T and C_Q', respectively, are plotted against angle of blade incidence in figures 7 and 8.

Reduction of the data from the airfoil tests requires an interpretation of the wind-tunnel jet boundary effects. A study of the data revealed that the interference of the balance shielding was appreciable and, in an attempt to evaluate this interference, the work of Tani and Taima (reference 5) on the boundary influence of partial enclosures consisting of circular arcs, was consulted. It appeared that the balance shielding had an effect equivalent to an arc enclosure of approximately $145°$, which results in a zero correction for induced drag and angle of attack but a balance alignment correction of about $0.30°$ due to the upward inclination of the air stream produced by the boundary. This alignment correction was, therefore, applied to the original force test data. The results were then corrected to infinite aspect ratio by the customary formulas (reference 6). However, a small asymmetry remained, the inverted tests giving slightly higher values of lift and drag, and it was therefore necessary to draw an average curve between the points. Figure 9 shows these final curves with the minimum drag coefficient subtracted from the total profile drag to give the profile-drag variation curve required for the determination of ϵ.

COMPARISON OF THEORY AND EXPERIMENT

Thrust.- The experimental values of the new thrust coefficient T_σ are plotted against θ_σ in figure 10.

This figure shows at once that the assumption of an infinite number of blades and the elimination of σ as an independent parameter are fully justified since the points for the four rotors of solidities 0.0424, 0.0636, 0.0849, and 0.1061 all fall very closely on a single curve with the exception of the high incidence values where the profile lift curve no longer approximates a straight line.

In figure 9 it will be seen that a mean value of the lift-curve slope for infinite aspect ratio is 5.75 per radian. Using this value in equation (14) the theoretical thrust curve, also shown in figure 10, was obtained and indicates a fairly good agreement between theory and experiment except for small values of θ_σ.

Torque.- In order to obtain a single curve to define
the static torque characteristics of the helicopter, it is
evident from equations (16) and (17) that we must plot
$Q_\sigma' = \left(Q_\sigma - \dfrac{\delta}{4\sigma^2}\right)$ vs. θ_σ. In figure 11, therefore, the ex-
perimental values Q_σ' are plotted against θ_σ and here
again we find that the points for the different rotors
fall on a single curve with the exceptions noted above for
thrust.

In order to obtain the theoretical curve, it is nec-
essary to determine the value of ϵ, the coefficient of
profile-drag variation. This value, as shown in figure 9,
is 0.75 at the Reynolds Number of the blade tips. This
figure shows also that the assumed parabolic variation of
profile drag is justified, at least for this Reynolds
Number.

Using the value of 0.75 the torque coefficient curve
was obtained as shown in figure 11. This curve falls be-
low the experimental curve, but by increasing ϵ to 1.25,
excellent agreement is obtained.

A careful analysis of the assumptions has revealed
that the only one which might account for the thrust and
torque discrepancies is that of neglecting the slipstream
contraction but further study is required on this point.

As a matter of interest, the experimental values of
thrust and torque are plotted against each other on loga-
rithmic paper in figure 12, and indicate that the follow-
ing simple relation holds quite closely for the model
tests:

$$Q_\sigma' = 0.72\, T_\sigma^{3/2}$$

The thrust and torque coefficients are also plotted on
rectangular coordinates in figure 13. These results show
that the theoretical values of thrust are constantly higher
than the experimental values although the curves are of the
same general shape. The approximate equation gives excel-
lent agreement with the experimental curve up to a Q_σ' of
about 5. Beyond this point the approximate values of
thrust exceed the experimental values by an increasing
amount.

ANALYSIS OF PARAMETERS

In the past the interpretation of helicopter airscrew-model data has been made difficult and uncertain because of large scale effects. The magnitude of these differences due to scale may be judged from figure 14, which gives the curves of figure of merit M vs. blade-angle factor θ_σ for both model and full-scale conditions. The solidity chosen $\sigma = 0.06$, is approximately a median value for existing helicopters and autogiros, and the method used to obtain the data for these curves will become apparent in the subsequent discussion. It should be noted that the Reynolds Number range of the blade tips of existing helicopters and autogiros is approximately 2.5×10^6 to 3.5×10^6.

Fortunately, the theoretical portion of this investigation has revealed the existence of certain parameters that are functions of scale and the values of these corresponding to any Reynolds Number may be obtained from suitable airfoil tests. These airfoil parameters are:

a_0 is the slope of lift curve for two-dimensional flow.

δ, minimum profile-drag coefficient.

ϵ, profile-drag variation coefficient

Lift-curve slope, a_0.- For two-dimensional flow the slope of the lift curve varies slightly with the Reynolds Number and also with thickness and camber as shown in reference 4. However, inspection of this reference and figure 9 of this report, indicates that $a_0 = 5.75$ very nearly for both model and full-scale Reynolds Number. Moreover, for different airfoil profiles within the conventional thickness and camber ranges, the variations in a_0 are negligible. Thus, no appreciable error may be expected in assuming $a_0 = \text{const.} = 5.75$.

This conclusion enables us to derive the full-scale curve of thrust coefficient T_σ vs. blade-incidence factor θ_σ. However, it should first be recalled that figure 10 shows an appreciable discrepancy between the theoretical and experimental curves for the constant incidence type of rotor for $\theta_\sigma < 3.5$. Consequently, for the sake

of accuracy, the faired experimental values should be used
over this range. For $\theta_\sigma > 3.5$ the theoretical values of
T_σ, equation (14) must be used since beyond this point
stalling of the model rotor blades begins to occur for the
rotor of solidity $\sigma = 0.0424$. In order to justify this
use of the theoretical values, one experimental point from
the single-blade rotor tests, $\sigma = 0.0212$, is plotted in
figure 10, and this falls very close to the theoretical
curve at $\theta_\sigma = 4.93$. In figure 15 the modified thrust co-
efficient curve thus obtained is plotted on logarithmic
coordinates since this form gives approximately constant
accuracy for reading values from the curves.

As the incidence of the blades is increased a point is
finally reached where the blades begin to stall. In the
experiments this condition could easily be detected by the
loud roaring noise that resulted. However, even before
the stall occurs the lift curve departs sufficiently from
a straight line to cause appreciable divergence from the
theory and it is, therefore, necessary to determine this
limiting value of blade incidence. Referring to equation
(7a), we note that

$$\varphi^2 = (\theta - \varphi) \frac{a_0 \sigma}{8x} = (\theta - \alpha)^2$$

or

$$\theta^2 - 2\theta \alpha + \alpha^2 - \frac{\alpha}{x} \frac{a_0}{8} = 0$$

and

$$\theta = \alpha + \sqrt{\frac{\alpha}{x} \frac{a_0 \sigma}{8}}$$

Inspection of the derivation leading to equation (8)
indicates that, for both constant-pitch and constant-inci-
dence rotors, stalling will first occur at the blade tips,
i.e., $x = 1$. Hence, the desired limiting value of tip
incidence is

$$\theta_0 = \alpha + \sqrt{\alpha \frac{a_0 \sigma}{8}}$$

where α is the absolute angle of attack (radians).

A study of the airfoil characteristics given in ref-
erence 4 shows that the value of α at which the profile-
lift curve departs noticeably from a straight line, is

about 14° for practically all airfoils having thickness
ratio not less than 0.09. Thus, for present full-scale
lifting airscrews, we may assume that

$$\theta_0 = 0.25 + \sqrt{0.25 - \frac{a_0}{\frac{\sigma}{8}}}$$

or

$$\theta_{\sigma_0} = \frac{0.25}{\sigma} + \sqrt{\frac{0.25}{\sigma} - \frac{a_0}{8}}$$

The limiting values of θ_{σ_0} derived from the above
equation are shown in figure 15 for different solidities
and are also indicated in all the figure-of-merit curves.

Profile-drag variation coefficient, ϵ.- In presenting
the experimental torque data in the form of the new coeffi-
cient Q_σ', mention has already been made of the fact that

$$Q_\sigma' = \left(Q_\sigma - \frac{\delta}{4\sigma^2}\right) = f(a_0, \theta_\sigma)$$

But Q_σ' is composed of two parts as indicated in equations
(16) and (17). These are the "induced torque" and the "pro-
file-variation torque," and in the latter the quantity ϵ
appears as a coefficient. The value of this coefficient
for the rotor-model tests was found to be 1.25 as shown in
figure 11, although the airfoil tests indicated a value of
0.75. (See fig. 9.) This discrepancy is partly due to the
lower Reynolds Number at which the inner portions of the
blades were operating and probably also to the large inward
radial velocity components near the tips that have been
neglected in the theory. To account for this difference,
we may write:

$$\epsilon = K\epsilon'$$

where ϵ is the profile torque variation coefficient

        ϵ', profile drag variation coefficient

   $K = 1.67$, correlation factor

Since no suitable full-scale test data on lifting airscrews
are known to the writers, we shall assume that K is in-
dependent of scale. On this basis the full-scale value of

ϵ may be estimated from the lower curve of figure 9 which was obtained from reference 4 at R.N. = 3.5 x 10^6 for the N.A.C.A. 0015 airfoil used in the rotor models. This value of ϵ' appears to be about 0.18 and hence $\epsilon = 0.30$ should be a fair representation of the coefficient for existing full-scale rotors.

In estimating the full-scale torque coefficient Q_σ', figure 11 indicates that the theoretical data may be expected to give good accuracy. Hence the theoretical values for the constant-incidence rotor have been computed using $\epsilon = 0.3$ and $a_o = 5.75$ and yield the torque curve Q_σ' vs. θ_σ given in figure 15.

Variations in ϵ with camber are greater than those with thickness but in general both are small enough to be neglected.

Minimum profile-drag coefficient, δ.- This coefficient appears in the form $-\dfrac{\delta}{4}\dfrac{}{\sigma^2}$ in equations (16) and (17) and is obviously constant for a given rotor. The term $-\dfrac{\delta}{4}\dfrac{}{\sigma^2}$ is the minimum torque and is obtained when the thrust is zero. The value of δ obtained from averaging the four rotor model tests was 0.0115 and from the airfoil tests was 0.0113, a surprisingly good agreement.

The determination of full-scale values of δ presents some difficulty due to lack of agreement between the results of different wind tunnels. Recent large-scale profile-drag tests made at the D.V.L. (reference 7), seem to indicate that the values of δ obtained in the N.A.C.A. variable-density tunnel (reference 4) are too high due to tip effect and relatively great surface roughness. Until such divergences can be reconciled, careful judgment will be required in the estimation of δ for a given airfoil.

Minimum profile drag is a function of camber as well as thickness, but since airfoils suitable for use in lifting airscrews must have small cambers to prevent undue blade twist and possible flutter, we may neglect this effect.

Figure-of-merit curves.- A study of the effects of varying the different parameters can be made with the aid of curves of figure of merit M, plotted against blade-incidence factor θ_σ. Recalling that

$$M = \frac{1}{2} \frac{T_\sigma^{3/2}}{Q_\sigma}$$

$$= \frac{1}{2} \frac{T_\sigma^{3/2}}{\frac{\delta}{4\sigma^2} + Q_\sigma{'}}$$

we note that $M = f\left(\epsilon, \frac{\delta}{4\sigma^2}, \theta_\sigma\right)$, assuming variations in a_0 to be negligible.

The effect of ϵ upon M for the constant-incidence rotor may be judged from figure 16, which was computed from the estimated full-scale data of table VII. Values of ϵ of 0.1, 0.3, and 0.5 and a range of θ_σ from zero to 9 are shown, and median values of the other parameters were used. In this and subsequent figures the curve of ideal figure of merit M_I, is included for comparison.

It is interesting to note that ϵ has practically no effect up to $\theta_\sigma = 1.5$. However, at $\theta_\sigma = 4.8$, which is the upper limit of $a_0 = 5.75$, for $\sigma = 0.06$ an appreciable divergence is evident. The curve $\epsilon = 0.1$ will doubtless never be reached unless very much larger rotors than now exist are developed, whereas $\epsilon = 0.5$ is representative of small rotors such as might be used as test models in a large wind tunnel.

In figure 17 similar curves are shown for $\delta = 0.006$, 0.009, and 0.012, computed for the median full-scale value $\epsilon = 0.3$. Here the lowest value of δ represents a large rotor with a thin blade profile, and the highest, a small rotor with a thick profile. The value $\delta = 0.009$ represents the probable full-scale median. Comparison of figures 16 and 17 shows that for $\theta_\sigma > 3.5$, ϵ has a greater effect on M than δ, whereas for $\theta_\sigma < 3.5$, the reverse is true.

An idea of the effect of blade twist on M can be obtained from figure 18 for the two cases $\theta = $ constant and $\theta = \frac{\theta_0}{x}$ (constant pitch). Since no suitable experimental data are available for the constant-pitch airscrew of constant chord and profile, it was necessary to compute the curves of figure 18 from the theoretical thrust and torque

equations. The _relative_ values of M for the two types
of blade should be given reliably by these curves. It
will be noted that the _percentage_ increase in M of the
constant-pitch rotor over that for the constant-incidence
rotor is greater for small values of θ_σ and the ratio of
the values of M_{max} is about 1.07.

The theoretical ideal figure of merit M_I, for the
constant-pitch rotor has already been shown to be a con-
stant and equal to unity. For the constant-incidence ro-
tor, M_I, is not exactly constant, but increases slowly
with θ_σ. This variation is so small, however, that M_I =
0.94 = constant may be considered a satisfactory repre-
sentation. The curve of M_I calculated from the modified
data of table VII is included in the figure and shows a
large deviation from this theoretical value at small val-
ues of θ_σ.

In connection with figure 18 it should, of course,
be kept in mind that the curve p = constant represents a
different blade twist for each value of θ_σ. If the blades
were merely turned as a whole without change of twist, the
values of M would lie somewhere between the two curves.

The foregoing analysis of the effect of changing the
blade parameters clarifies somewhat this phase of the lift-
ing airscrew problem. However, there still remains a need
for more consistent and extensive large-scale data on the
characteristics of airfoils suitable for lifting airscrews.

Having established full-scale values of the parameters,
it is now possible to construct a general figure-of-merit
chart from which, together with figure 15, the hovering
characteristics of any constant-chord and incidence-lifting
airscrew can be quickly derived. This chart is shown in
figure 19 and is based on the following parametric values:

$$a_o = 5.75$$

$$\epsilon = 0.3$$

$$\delta = 0.006 \text{ and } 0.012$$

$$\frac{\delta}{4\sigma^2} = 0 \text{ to } 3.2$$

The narrow cross-hatched band in this figure represents the region of M_{max} (limit of $a_0 = 5.75$) for different values of δ and σ. This region indicates the significant fact that the "lifting efficiency" of all rotors of this type will be very nearly 0.80 with extreme deviations of ±0.04. The most efficient rotor for hovering flight should obviously have a large solidity and a small-blade profile drag, but the small solidity rotors essential for efficient forward motion would not be greatly inferior when hovering.

As a matter of theoretical interest the curves of M_I and $\dfrac{\delta}{4\sigma^2} = 0$ are included in this chart, and all the curves are carried up to $6_\sigma = 9$ for the same reason. In this connection it will be noted that the full-scale limit of $a_0 = 5.75$, i.e., $\alpha = 14^\circ$, enables the maximum value of M to be very nearly reached in most cases.

HOVERING-FLIGHT PERFORMANCE

The hovering-flight performance characteristics of any helicopter may be readily determined by the simple method developed by Glauert in reference 2. This method has been somewhat modified by the writers and has been reduced to two simple charts from which altitude performance can be easily calculated.

The figure of merit may be expressed as

$$M = \frac{1}{2} \frac{T}{\Omega Q} \sqrt{\frac{2T}{\rho \pi R^2}} = \frac{T_\sigma^{3/2}}{Q_\sigma} \tag{19}$$

where ΩQ is the power required. And by analogy we may write:

$$N = \frac{1}{2} \frac{W}{P'} \sqrt{\frac{2}{\rho \pi} \frac{W}{R}} \tag{20}$$

where $P' = \eta P$ is the power available at rotor

                P, power of motor

                η, efficiency of drive system

and   W, weight

The factor η is very nearly unity for ordinary propulsive airscrews, but for the lifting airscrew it will vary considerably, depending upon the type of drive used.

From the above expressions, it is at once apparent that for hovering flight at a given altitude

$$\frac{M}{N} = \frac{P'}{\Omega Q}$$

which is the ratio of power available to power required, and that hovering flight is therefore possible only when $M \geq N$.

The expression for M also shows that for a given thrust, the power required will be inversely proportional to the radius R of the rotor and, consequently, for maximum economy the rotor should be as large as possible.

Using the subscript zero to denote sea-level conditions,

$$\frac{M}{N_0} = \frac{P'_0}{P'} \sqrt{\frac{\rho_0}{\rho}} = f_1(H)\, f_2(H) \qquad (21)$$

and adopting the relationships for power and density variation with altitude given by Diehl in reference 8, figure 20 has been prepared by plotting M/N_0 vs. H.

Since for hovering flight $M = N$, the following relationships at sea level may be obtained from equation (20):

$$\left(\frac{W}{MP'_0}\right) = \sqrt{\frac{2\rho_0}{\frac{W}{\pi R^2}}} \qquad (22)$$

In this equation two loading factors are apparent and these will be designated as

$$\left(\frac{W}{MP'_0}\right) = l_p, \quad \text{the "ideal effective" power loading}$$

$$\left(\frac{W}{\pi R^2}\right) = l_s, \quad \text{the rotor disk loading}$$

Thus equation (22) becomes

$$l_p = \sqrt{\frac{2\rho_0}{l_s}} \qquad\qquad (23)$$

and this relationship is plotted in figure 21 in terms of engineering units.

The concept of an "ideal effective" power loading is useful in that it makes possible the simple relationship of equation (23) and the single curve of figure 21, which is perfectly general. The form of this fictitious power loading shows that it merely signifies a higher value for actual rotors and, therefore, an inferior performance as compared with the ideal case of $M_I = 1$.

The power ratio for hovering flight may now be expressed in terms of the loading factors as follows:

$$\frac{M}{N_0} = \frac{1}{l_p}\sqrt{\frac{2\rho_0}{l_s}} \qquad\qquad (24)$$

Determination of the rotor tip speed can be made quite simply. If we write that

$$\frac{T}{P'} = \frac{W}{P'} = \frac{\sigma\, T_\sigma^{3/2}}{\Omega R\, Q_\sigma}$$

and

$$\left(\frac{W}{MP'}\right) = \frac{\sigma\, T_\sigma}{M\,\Omega R\, Q_\sigma}$$

but remembering that $M = \frac{1}{2}\dfrac{T_\sigma^{3/2}}{Q_\sigma}$, we obtain

$$\Omega R = \frac{2}{\sigma\, l_p\, T_\sigma^{1/2}} \qquad\qquad (25)$$

and since for a given rotor and blade angle, σ and T_σ are constant, the tip speed is inversely proportional to the "ideal effective" power loading.

Altitude performance calculations.- The following simple expressions, converted to engineering units, enable the calculation of the performance parameters by means of which, with the curves of figures 20 and 21, the hovering performance characteristics of any helicopter may be determined.

$$L_P = \left(\frac{W}{M \eta P}\right) \text{ in lb. per hp.} \tag{A}$$

$$L_S = \left(\frac{W}{\pi R^2}\right) \text{ in lb. per sq.ft.} \tag{B}$$

$$\frac{M}{N_0} = \frac{38}{L_P L_S^{1/2}} \tag{C}$$

$$\Omega R = \frac{1100}{L_P (\sigma T_\sigma)^{1/2}} \text{ in ft. per sec.} \tag{D}$$

The following example is included to show how the method is used. Since adequate data on recent constant-chord helicopters are not available, the C 30 autogiro has been selected for this purpose. This machine has the following approximate characteristics:

Rotor radius, R . . . . 18.5 ft.

Normal loaded weight, W . . . . . 1,800 lb.

Assumed effective power, P' . . . . 120 hp.

Solidity, σ 0.05

Minimum profile-drag coefficient, δ 0.008

1. The value of M can be determined from figure 19, since $\frac{\delta}{4 \sigma^2} = 0.8$, and is seen to be 0.81 at a blade incidence factor of $\theta_\sigma = 7$ or a blade incidence of

$$\theta = 57.3 \sigma \theta_\sigma$$

$$= 20.1^\circ$$

2. The sea-level minimum loading factors will be

$$L_{P_1} = \left(\frac{1800}{0.81 \times 120}\right) = 18.5 \text{ lb. per hp.}$$

$$L_{S_1} = \frac{1800}{\pi \, 18.5^2} = 1.68 \text{ lb. per sq.ft.}$$

3.   The power ratio from equation (C) is

$$\frac{M}{N_0} = \frac{38}{18.5 \times (1.68)^{1/2}} = 1.59$$

4.   The absolute ceiling for hovering flight can be obtained immediately from figure 20, as indicated by the dotted lines, and is

$$H_c = 8,700 \text{ feet for } \frac{M}{N_0} = 1.59$$

5.   The maximum load that can be sustained at sea level (neglecting ground effect) is obtained by noting in figure 21 that the upper limit of disk loading L_{s_2}, which occurs at $L_{p_1} = 18.5$, is 4.2 and, therefore,

$$W_{max} = \frac{L_{s_2}}{L_{s_1}} W_{min} = \frac{4.20}{1.68} \times 1,800 = 4,500 \text{ lb.}$$

6.   The minimum rotor power required at sea level (neglecting ground effect) is also obtained from figure 21 in a similar fashion by noting that the upper limit of power loading L_{p_2}, which occurs at $L_{s_1} = 1.68$, is 29.3, and therefore,

$$P'_{min} = \frac{L_{p_1}}{L_{p_2}} P'_{max} = \frac{18.5}{29.3} 120 = 76 \text{ hp.}$$

7.   The rotor tip speeds corresponding to the maximum and minimum loadings are obtained from equation (D). The thrust coefficient must first be obtained from figure 15 and for $\sigma = 0.05$ is found to be 9.0. Thus, for $L_{p_1} = 18.5$ corresponding to $W_{max} = 4,500$ pounds.

$$\Omega R = \frac{1100}{18.5 \times 0.05 \times 9\frac{1}{2}} = 396 \text{ ft. per sec.}$$

and for $L_{p_2} = 29.3$ corresponding to $W_{min} = 1,800$ pounds.

$$\Omega R = \frac{1100}{29.3 \times 0.05 \times 9\frac{1}{2}} = 250 \text{ ft. per sec.}$$

CONCLUSIONS

The following conclusions can be drawn from the re-sults of this investigation on the lifting airscrew:

1. The vortex concept used in deriving the expression for the axial induced velocity yields results identical with those obtained by the use of the momentum equation.

2. The experiments amply verify the theoretical con-clusion that the solidity can be eliminated as a separate parameter insofar as thrust and torque are concerned if the minimum torque is subtracted from the total torque.

3. The experiments verify the assumption that for a given solidity the results are independent of the number of blades.

4. The theoretical equations disclose the existence of certain airfoil parameters with the aid of which scale effect can be accounted for quite simply.

5. General full-scale curves of thrust and torque for the constant chord and incidence rotor can be estimated with reasonable confidence by a judicious combination of the theoretical and experimental data of this report.

6. In general, it appears that the optimum figure of merit for the full-scale constant chord and incidence rotor may be taken as 0.80, and for the constant chord and pitch rotor as 0.85 with a probable maximum error for extreme cases of not more than ±0.04.

7. Helicopter hovering-flight performance can be rapid-ly determined by means of the two simple ceiling and loading charts of this report when the figure of merit and thrust coefficient are known.

ACKNOWLEDGMENTS

Daniel Guggenheim School of Aeronautics,
Georgia School of Technology,
Atlanta, Georgia, June 9, 1937.

REFERENCES

1. Bréguet, Louis: The Gyroplane – Its Principles and
       Its Possibilities. T.M. No. 816, N.A.C.A., 1937.

2. Glauert, H.: On the Vertical Ascent of a Helicopter.
       R. & M. No. 1132, British A.R.C., 1927-1928.

3. Prandtl, L., and Tietjens, O. G.: Fundamentals of
       Hydro- and Aeromechanics. McGraw-Hill Book Co.,
       Inc., New York, 1934.

4. Jacobs, Eastman N., Ward, Kenneth E., and Pinkerton,
       Robert M.: The Characteristics of 78 Related Air-
       foil Sections from Tests in the Variable-Density
       Wind Tunnel. T.R. No. 460, N.A.C.A., 1933.

5. Tani, I., and Taima, M.: Two Notes on the Boundary In-
       fluence of Wind Tunnels of Circular Cross Section.
       Report No. 121, Aeronautical Research Institute,
       Tokyo Imperial University, vol. 10, no. 3.

6. Jacobs, Eastman N., and Abbott, Ira H.: The N.A.C.A.
       Variable-Density Wind Tunnel. T.R. No. 416, N.A.C.A.,
       1932.

7. Doetsch, H.: Profilwiderstandmessungen im Grossen Wind-
       Kanal der D.V.L. Luftfahrtforschung, April 20,
       1937.

8. Diehl, W. S.: Engineering Aerodynamics, revised edi-
       tion. The Ronald Press Co., New York, 1936.

TABLE I

Helicopter Model Tests - Static Thrust

2-blade rotor, $\sigma = 0.0424$

$\epsilon°$	C_T	C_Q	C_Q'	T_σ	Q_σ	Q_σ'	ϵ_σ
0	0	0.000108	0	0	1.41	0	0
1	.000280	.000111	.000003	.156	1.45	.04	.41
2	.000873	.000125	.000017	.485	1.64	.23	.82
4	.00248	.000191	.000083	1.38	2.50	1.09	1.65
6	.00442	.000316	.000208	2.46	4.14	2.73	2.47
8	.00650	.000494	.000386	3.61	6.47	5.06	3.29
10	.00847	.000691	.000583	4.70	9.06	7.65	4.11
12	.00990	.000878	.000770	5.50	11.50	10.09	4.94

TABLE II

Helicopter Model Tests - Static Thrust

3-blade rotor, $\sigma = 0.0636$

$\epsilon°$	C_T	C_Q	C_Q'	T_σ	Q_σ	Q_σ'	ϵ_σ
0	0	0.000185	0	0	0.71	0	0
2	.00102	.000206	.000021	.252	.80	.09	.55
4	.00298	.000300	.000115	.736	1.16	.45	1.10
6	.00548	.000474	.000289	1.35	1.84	1.13	1.64
8	.00833	.000735	.000550	2.06	2.85	2.14	2.20
10	.01125	.001048	.000863	2.78	4.06	3.35	2.74
12	.01370	.001357	.001172	3.38	5.26	4.55	3.29

TABLE III

Helicopter Model Tests — Static Thrust

4-blade rotor, $\sigma = 0.0849$

θ°	C_T	C_Q	C_Q'	T_{σ}	Q_{σ}	Q_{σ}'	θ_{σ}
0	0	0.000268	0	0	0.44	0	0
1	.000287	.000274	.000006	.040	.45	.01	.21
2	.001042	.000300	.000032	.145	.49	.05	.41
3	.00214	.000338	.000070	.297	.55	.11	.62
4	.00338	.000410	.000142	.469	.67	.23	.82
5	.00473	.000499	.000231	.655	.82	.38	1.03
6	.00645	.000620	.000352	.895	1.01	.57	1.24
7	.00792	.000743	.000475	1.10	1.21	.77	1.44
8	.00981	.000920	.000652	1.36	1.50	1.06	1.65
9	.01182	.001162	.000894	1.64	1.90	1.46	1.85
10	.01382	.001395	.001127	1.92	2.28	1.84	2.06
11	.01596	.00171	.00144	2.21	2.79	2.35	2.26
12	.01745	.00191	.00164	2.42	3.12	2.68	2.47

TABLE IV

Helicopter Model Tests – Static Thrust

5-blade rotor, $\sigma = 0.1061$

θ°	C_T	C_Q	$C_Q{}'$	T_{σ}	Q_{σ}	$Q_{\sigma}{}'$	θ_{σ}
0	0	0.000238	0	0	0.200	0	0
2	.001181	.000270	.000032	.105	.226	.026	.33
4	.00362	.000396	.000158	.322	.332	.132	.66
6	.00694	.000680	.000442	.616	.57	.37	.99
8	.01103	.001086	.000848	.981	.91	.71	1.32
10	.01548	.001635	.001397	1.373	1.37	1.17	1.64
12	.0200	.00228	.00204	1.776	1.91	1.71	1.97

TABLE V

N.A.C.A. 0015 Profile Characteristics

6- by 72-inch airfoil   R.N. = 242,000

(Position A)

α_∞	c_L	c_{D_0}	Δc_{D_0}
12.65	0.873	0.0911	0.0798
11.55	.906	.0504	.0391
10.60	.899	.0383	.0270
8.70	.830	.0284	.0171
6.95	.711	.0222	.0109
5.30	.534	.0172	.0059
3.65	.351	.0131	.0018
1.95	.185	.0113	0
.25	.026	.0113	0
-1.45	-.138	.0102	-.0011
-3.10	-.302	.0136	.0023
-4.75	-.501	.0165	.0052
-6.40	-.693	.0205	.0092
-8.10	-.821	.0265	.0152
-9.95	-.915	.0350	.0237
-10.90	-.948	.0413	.0300
-11.90	-.939	.0710	.0607

TABLE VI

N.A.C.A. 0015 Profile Characteristics

6- by 72-inch airfoil   R.N. = 242,000

(Position B)

α_∞	c_L	c_{D_0}	Δc_{D_0}
12.00	0.955	0.0548	0.0435
11.00	.944	.0387	.0274
10.05	.909	.0331	.0218
8.25	.819	.0262	.0149
6.55	.663	.0210	.0097
4.90	.475	.0160	.0047
3.20	.304	.0132	.0019
1.55	.143	.0117	.0004
-.20	-.012	.0113	0
-1.85	-.174	.0121	.0008
-3.55	-.351	.0141	.0028
-5.15	-.561	.0177	.0064
-6.80	-.734	.0226	.0113
-8.60	-.831	.0286	.0173
-10.50	-.903	.0397	.0284
-11.45	-.910	.0533	.0420
-12.55	-.870	.0968	.855

TABLE VII

Helicopter Static Thrust

Full-scale data (est.)

$\theta = \text{const.}, \quad B = \infty, \quad a_o = 5.75$

θ_σ	T_σ	Coeff. of ϵ	Q_{σ_i}	Q_σ' $\epsilon = 0.3$	M_I
0	*0	0	0	0	→
.5	*.212	.005	.072	.074	0.680
1	*.638	.040	.341	.353	.748
2	*1.83	.265	1.42	1.50	.874
3	*3.20	.754	3.13	3.36	.914
4	4.65	1.54	5.38	5.84	.930
5	6.14	2.67	8.09	8.89	.936
6	7.64	3.70	11.28	12.39	.936
7	9.18	5.33	14.84	16.44	.936
8	10.74	8.13	18.30	20.74	--
9	12.34	10.71	23.05	26.25	.938

*Points taken from faired experimental data on four rotors.

TABLE VIII

Helicopter Theory - Static Thrust

$\theta = \text{const.}, \qquad B = \infty, \qquad a_o = 5.75$

$\epsilon = 0.3, \qquad\qquad \dfrac{\delta}{4\sigma^2} \neq 0.6$

θ_σ	T_σ	Coeff. of ϵ	Q_{σ_i}	$Q_\sigma{}'$ $\epsilon = 0.3$	Q_σ $\dfrac{\delta}{4\sigma^2} = 0.6$	M	M_I
0	0	0	0	0	0.600	0	
.5	.263	.005	.072	.074	.674	.100	0.938
1	.739	.040	.341	.353	.953	.334	.935
2	1.92	.265	1.42	1.50	2.10	.634	.937
3	3.26	.754	3.13	3.36	3.96	.745	.943
4	4.67	1.54	5.38	5.84	6.44	.785	.940
5	6.14	2.67	8.09	8.89	9.49	.807	.945
6	7.64	3.70	11.28	12.39	12.99	.813	.938
7	9.18	5.33	14.84	16.44	17.04	.816	.937
8	10.74	8.13	18.30	20.74	21.34	—	—
9	12.34	10.71	23.05	26.25	26.85	.806	.939

TABLE IX

Helicopter Theory – Static Thrust

$$p = \text{const.}, \quad B = \infty, \quad a_0 = 5.75$$

$$\epsilon = 0.3 \qquad \frac{\delta}{4\sigma^2} = 0.6$$

θ_{σ_0}	T_σ	Coeff. of ϵ	Q_{σ_i}	Q_σ $\epsilon = 0.3$	Q_σ $\frac{\delta}{4\sigma^2} = 0.6$	M
0	0	0	0	0	0.600	0
.5	.475	.013	.159	.163	.763	.214
1	1.259	.093	.706	.734	1.334	.521
2	3.18	.610	2.84	3.02	3.62	.782
3	5.30	1.70	6.12	6.63	7.23	.843
4	7.53	3.44	10.39	11.42	12.02	.859
5	9.85	5.87	15.52	17.28	17.88	.865
6	12.20	9.00	21.40	24.10	24.70	.865
7	14.61	12.93	28.00	31.88	32.48	.860
8	17.04	17.60	35.3	40.58	41.16	.856
9	19.51	23.00	43.1	50.00	50.60	.851
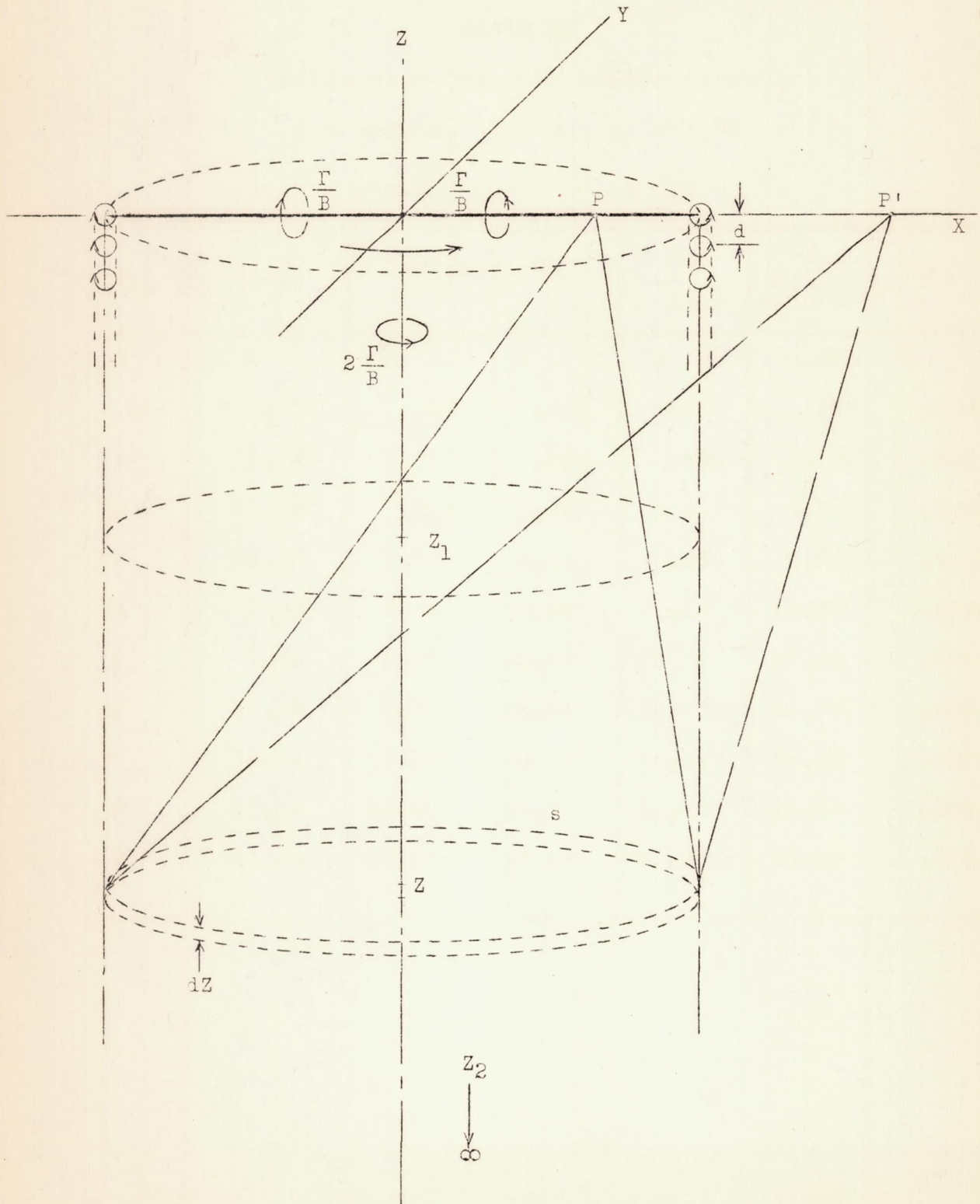
Figure 1
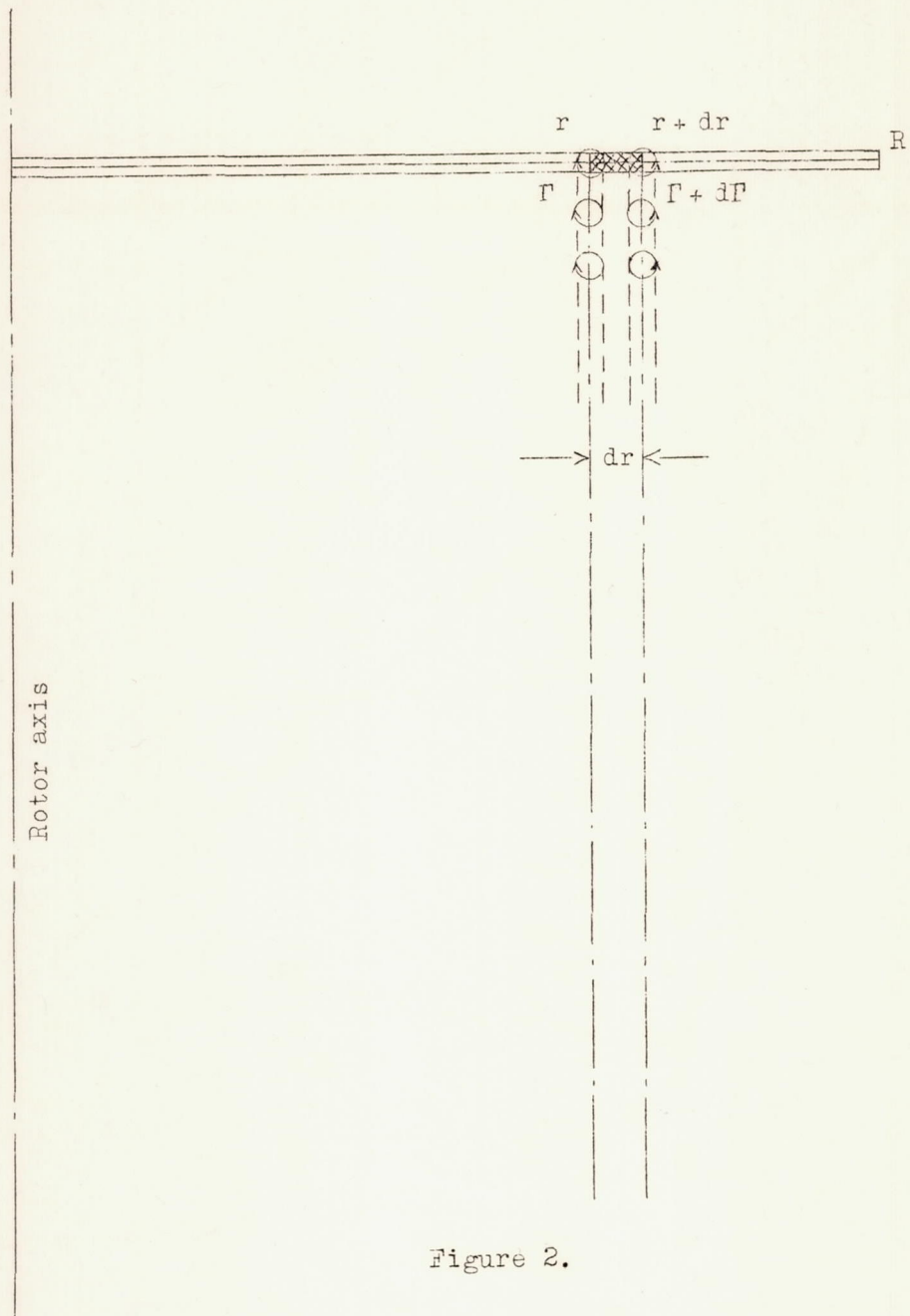
Figure 2.
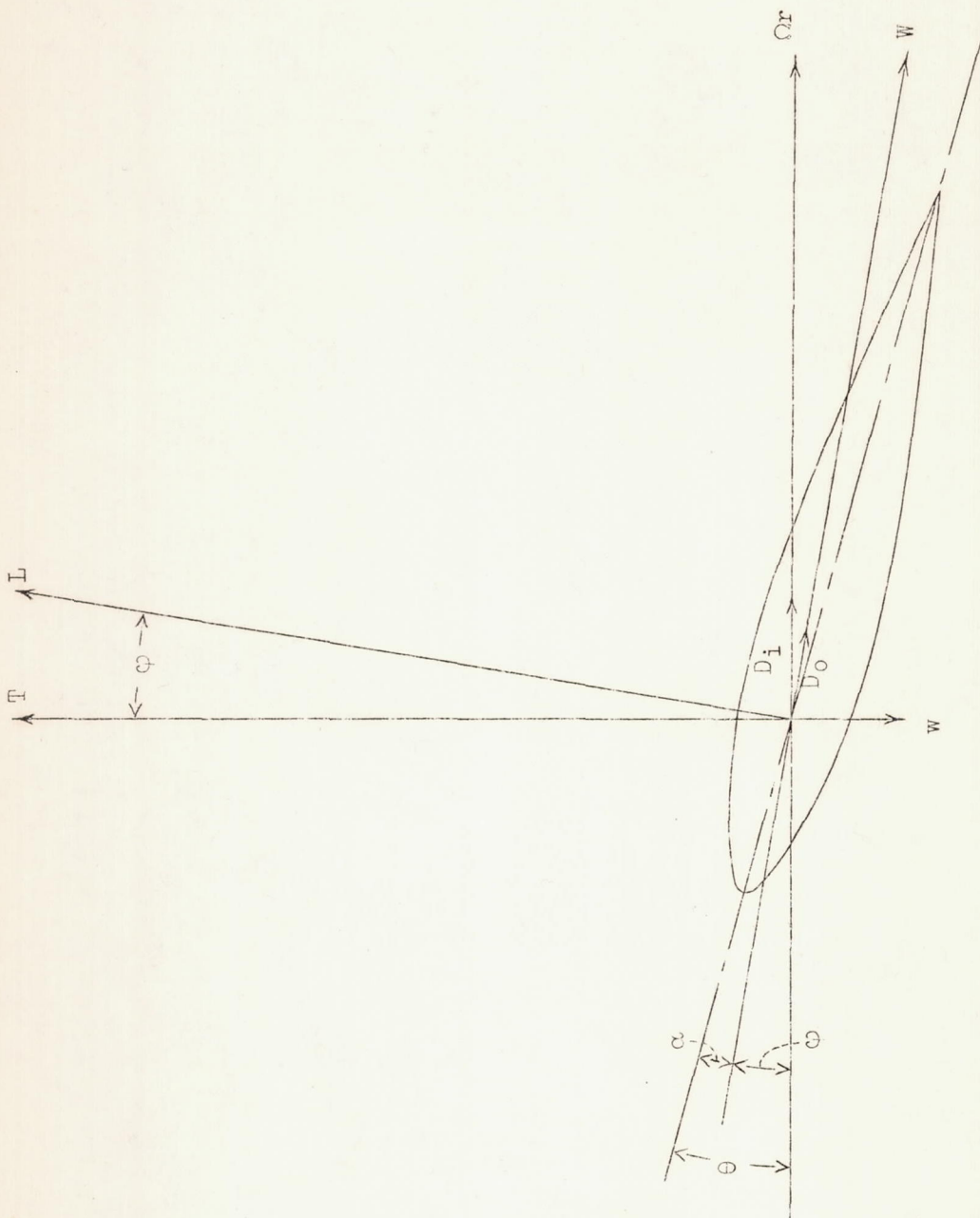
Figure 3.
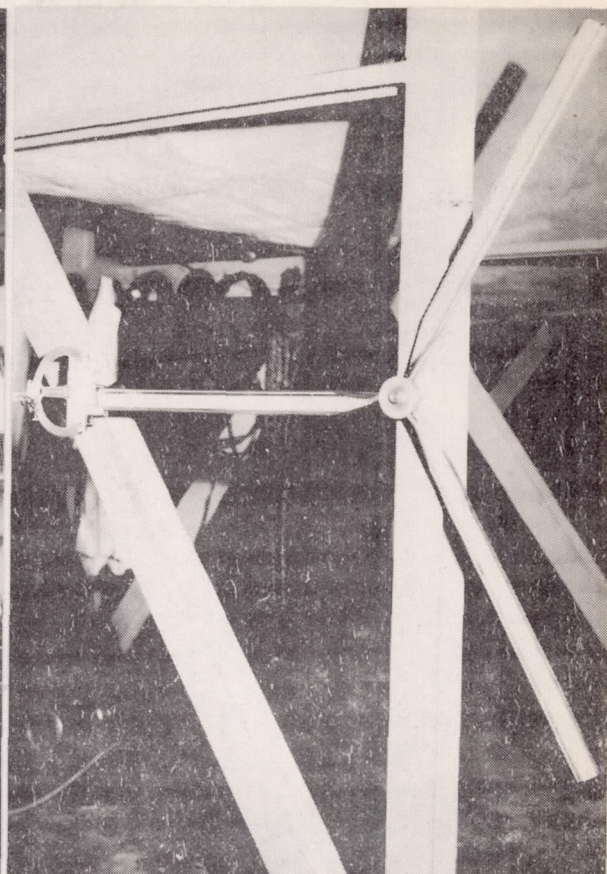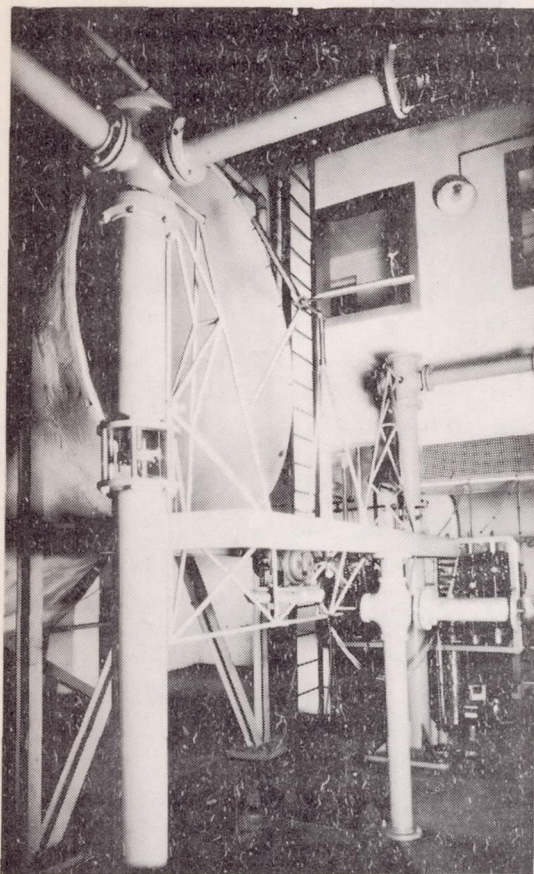
Figure 4.- Three-bladed rotor mounted   Figure 5.- Rotor model mounted on blade
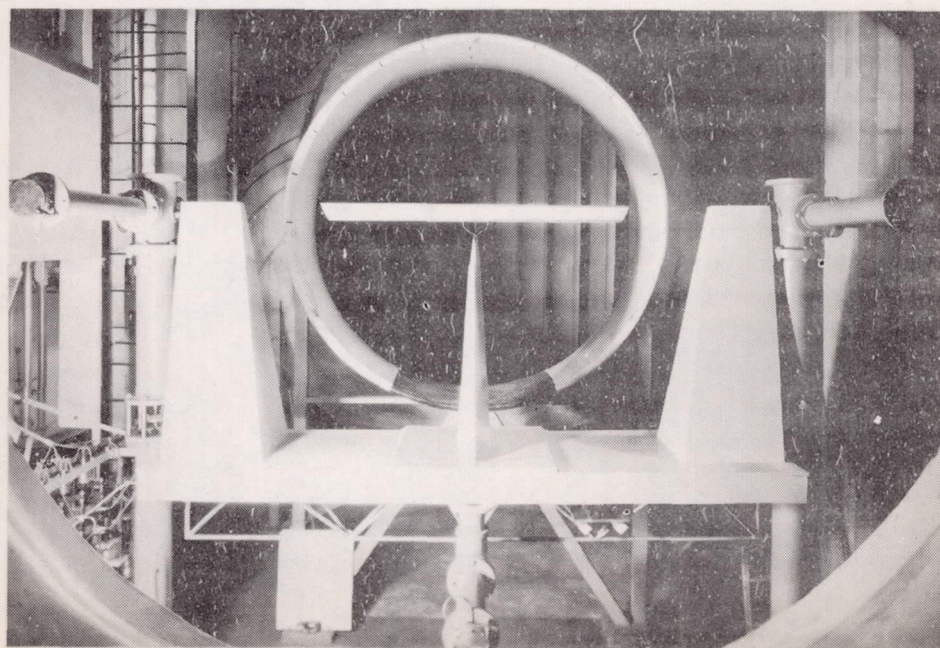   on wind tunnel balance.   incidence jig.

Figure 6.- Upstream view of airfoil model mounted for force tests in
           9 ft. wind tunnel.

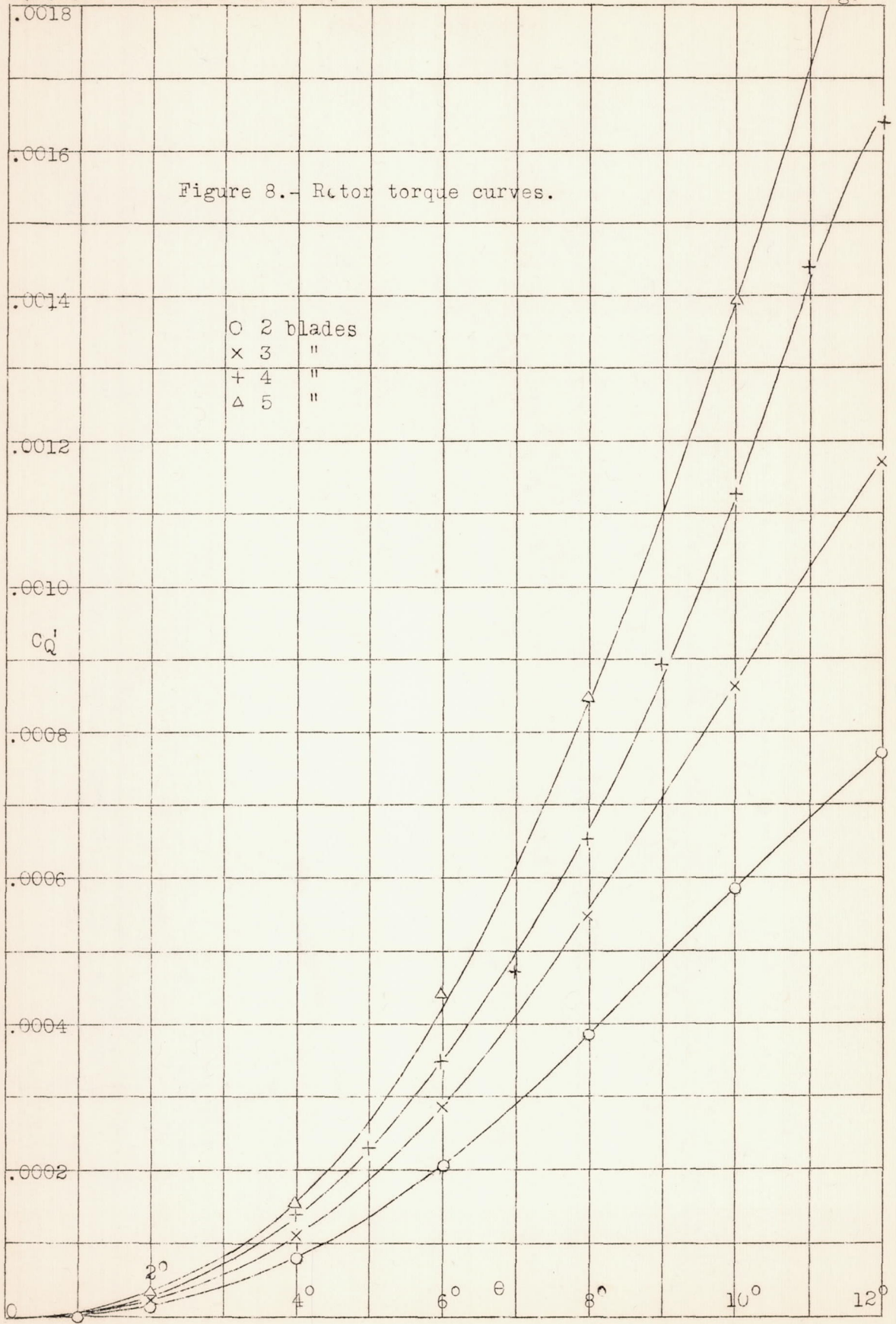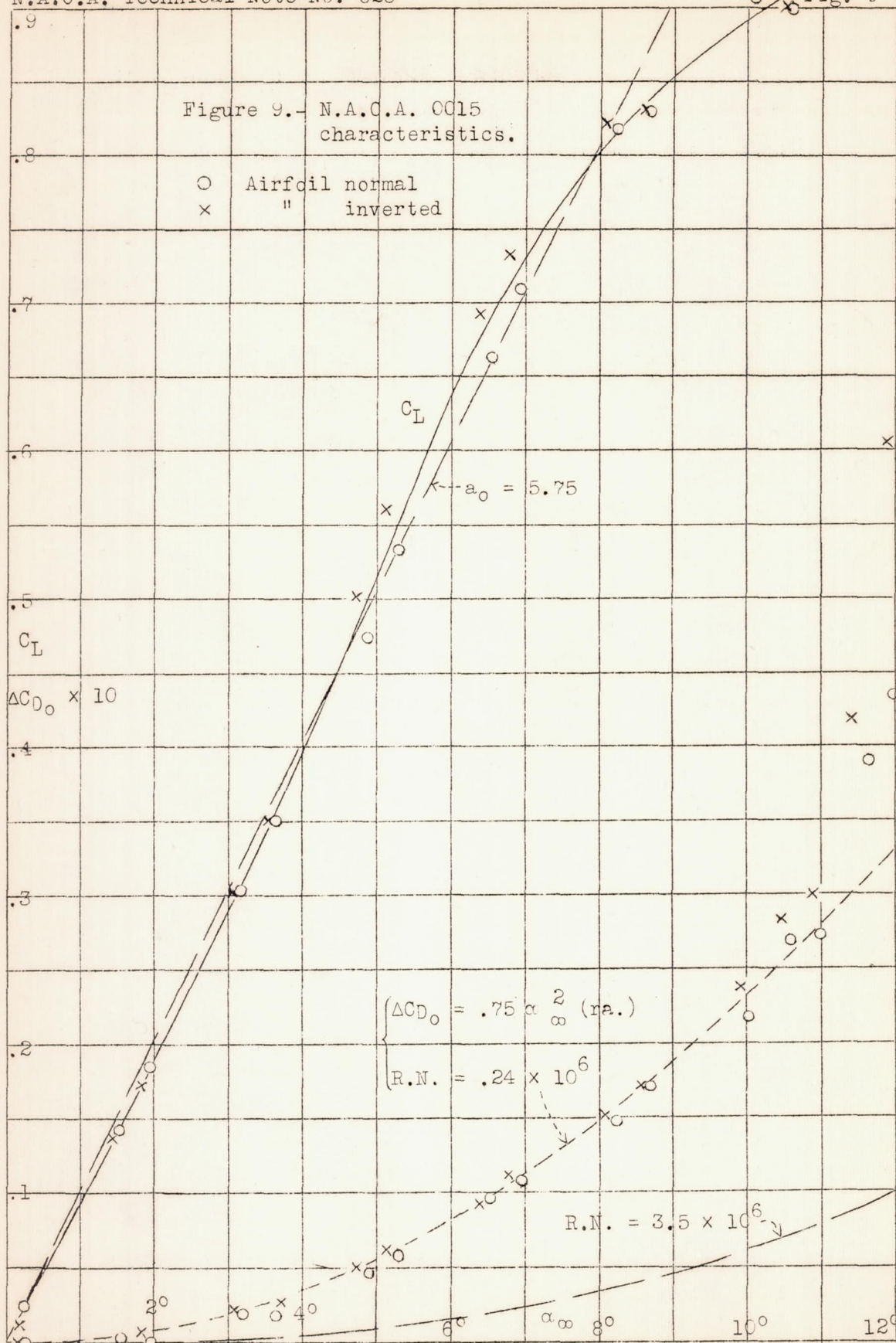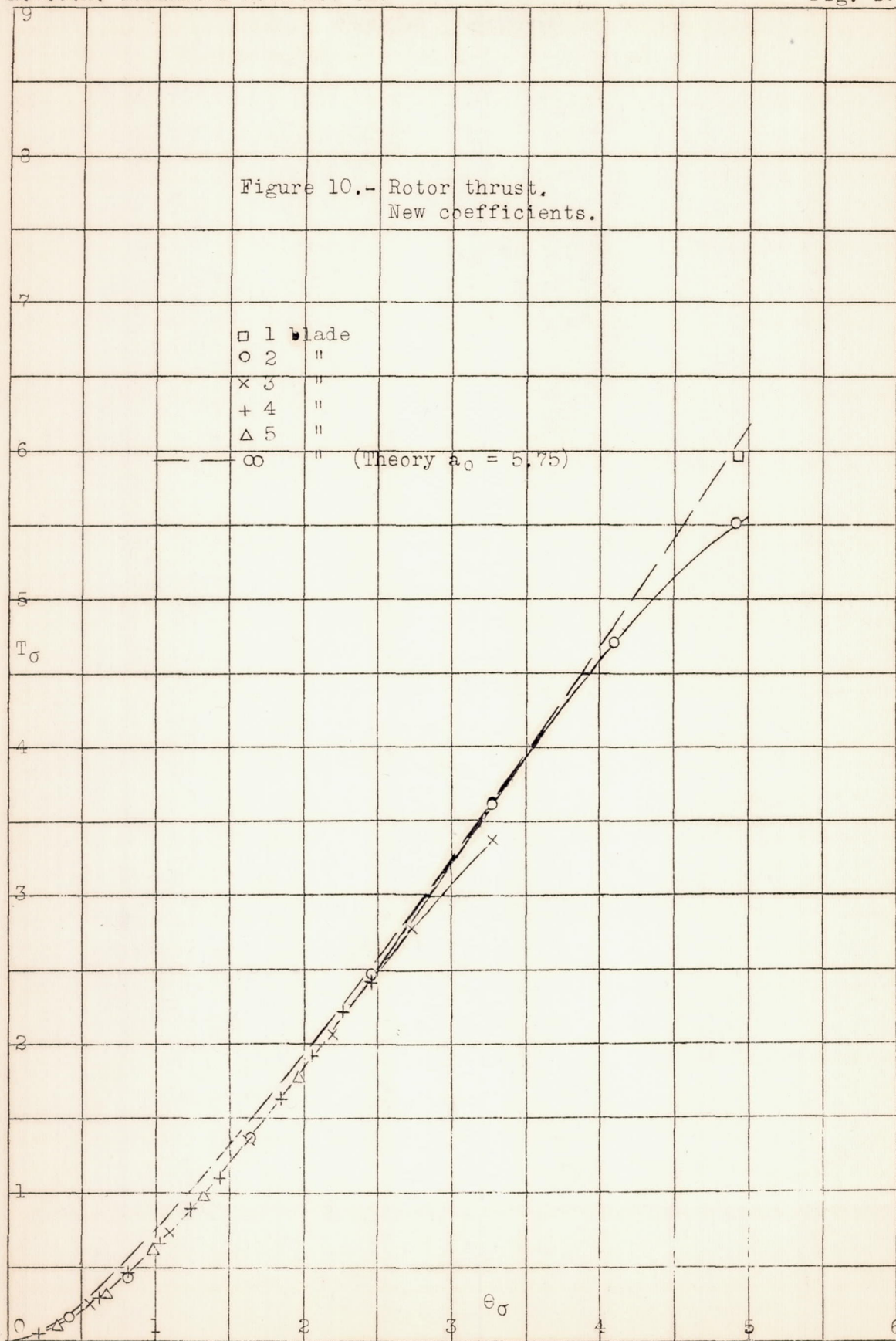Figure 7.- Rotor thrust curves.
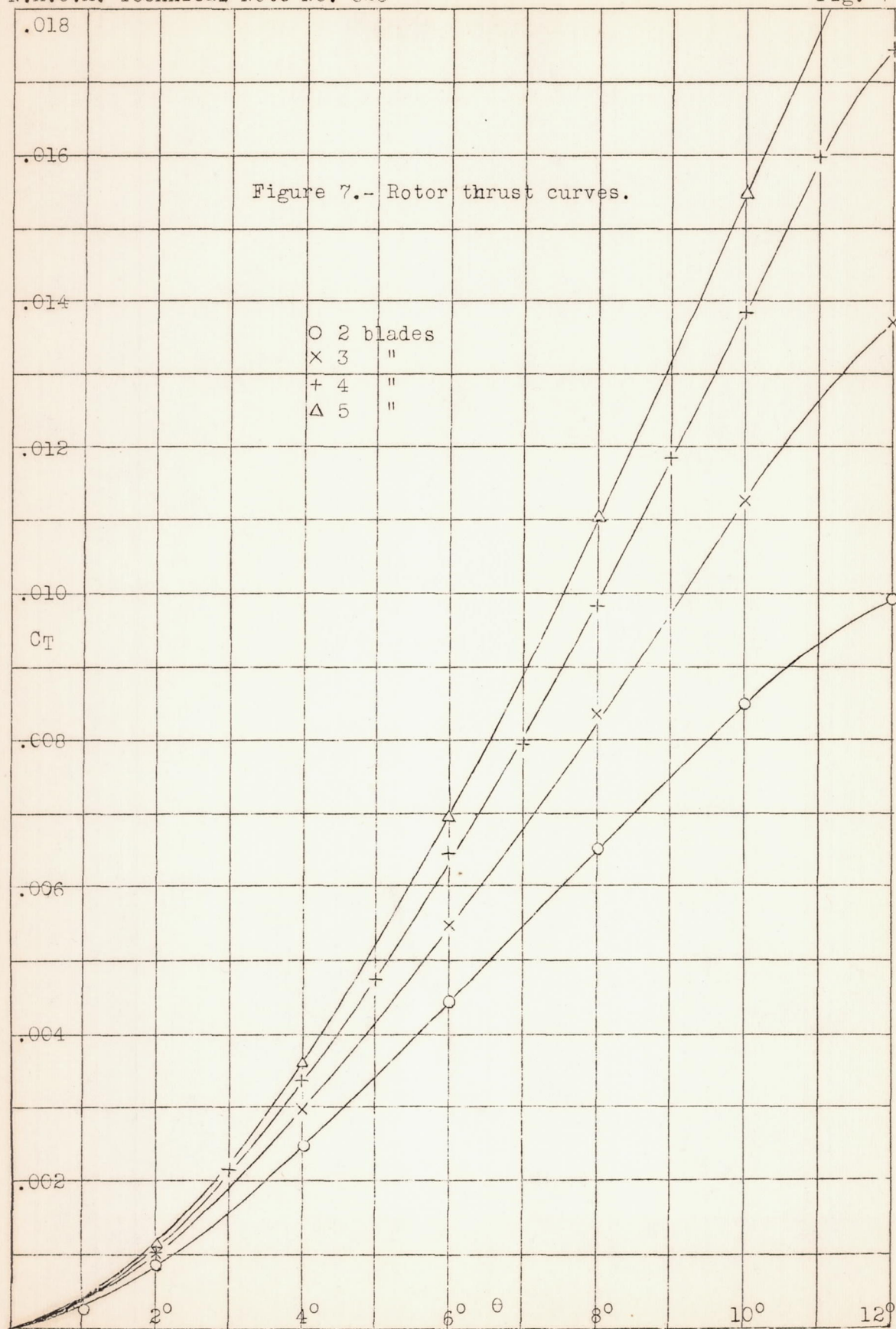
Figure 8.— Rotor torque curves.

C_Q'

○ 2 blades
× 3 "
+ 4 "
△ 5 "

θ

Figure 9.- N.A.C.A. 0015
characteristics.

○   Airfoil normal
×   "   inverted

C_L

×--a_0 = 5.75

C_L

$\Delta C_{D_0} \times 10$

ΔC_{D_0} = .75 a_∞^2 (ra.)

R.N. = .24 × 10^6

R.N. = 3.5 × 10^6

$2°$ $4°$ $6°$ α_∞ $8°$ $10°$ $12°$

Figure 10.- Rotor thrust.
New coefficients.

□ 1 blade
○ 2   "
× 3   "
+ 4   "
△ 5   "
— ∞   "   (Theory $a_0 = 5.75$)

T_σ

θ_σ

○   2 blades
×   3   "
+   4   "
△   5   "
———   ∞   "   (theory $\epsilon = 1.25$)
—·—   ∞   "   (theory $\epsilon = .75$)

Figure 11.- Rotor torque.
New coefficients.

$$Q'_\sigma = 0.72\ T_\sigma^{3/2}$$

○   2 blades
×   3   "
+   4   "
△   5   "
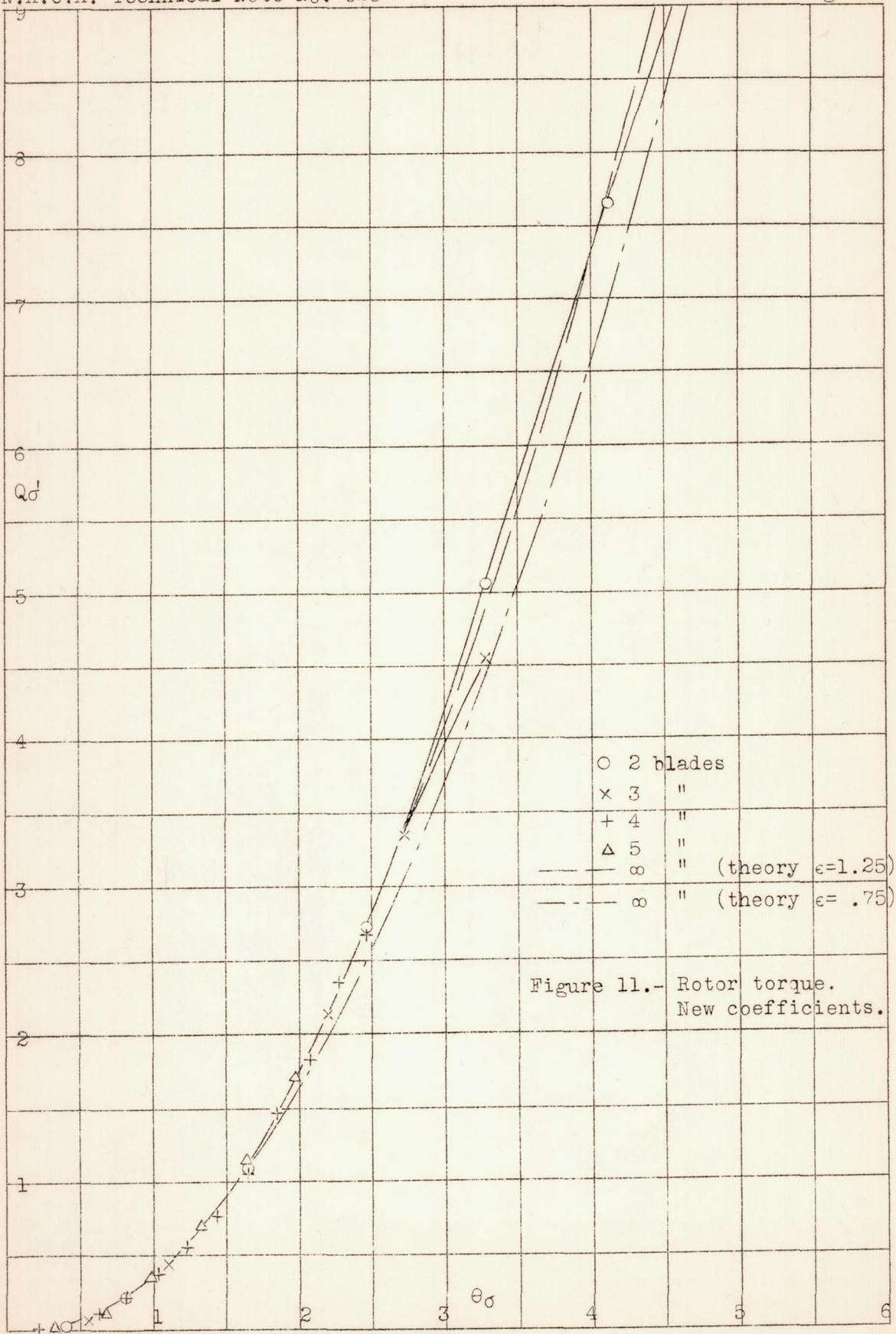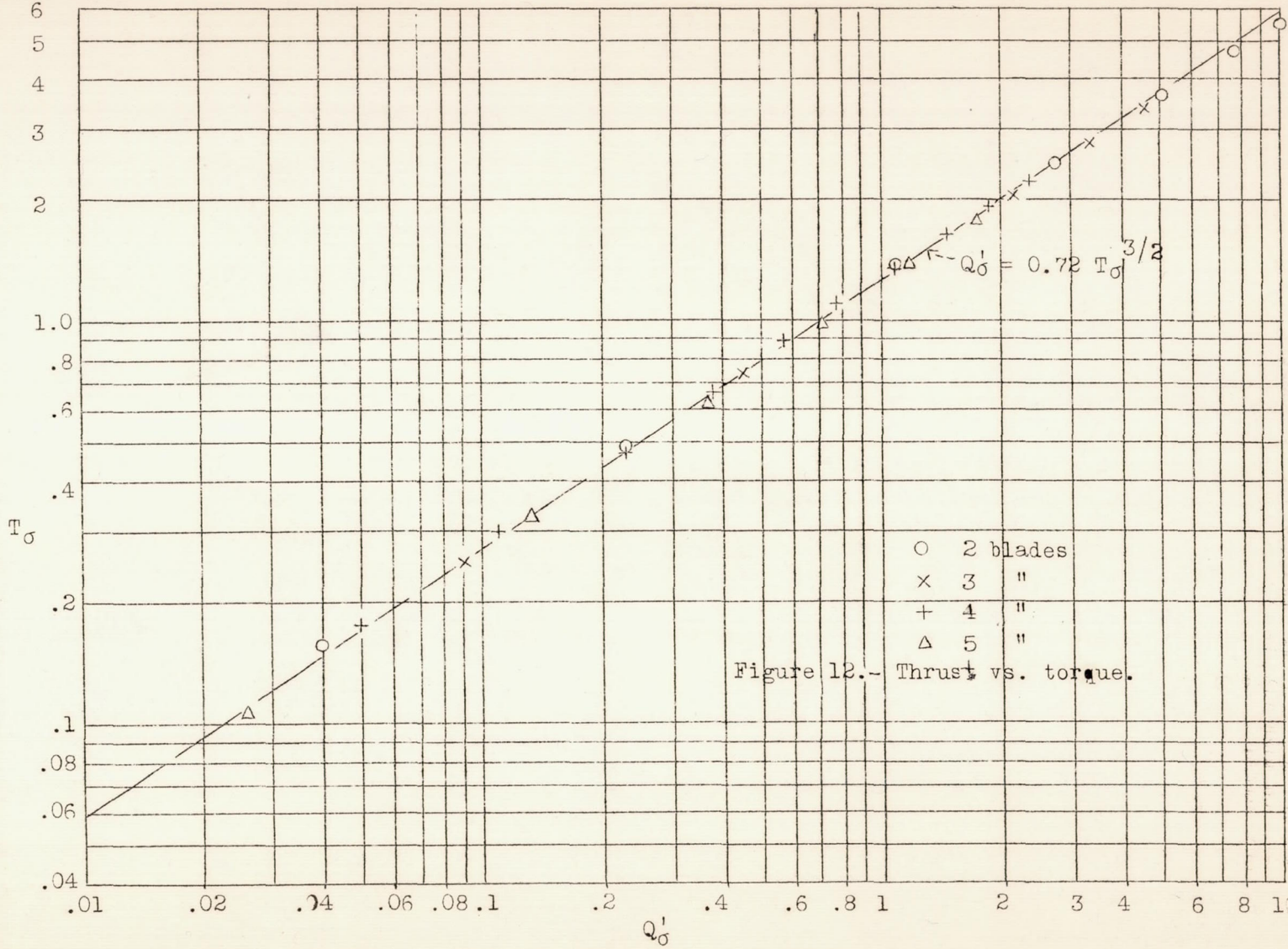
Figure 12.- Thrust vs. torque.

Fig. 12

2 blades
3   =
4   =
5   =
8   =   (theory)

O
×
+
△
— · —

$Q'_\sigma = 0.72\ T_\sigma^{3/2}$

Figure 13.- Thrust vs. torque.

Full scale R.N. = 3.5×10^6

Limit a_o = 5.75

Model R.N. = $.24 \times 10^6$
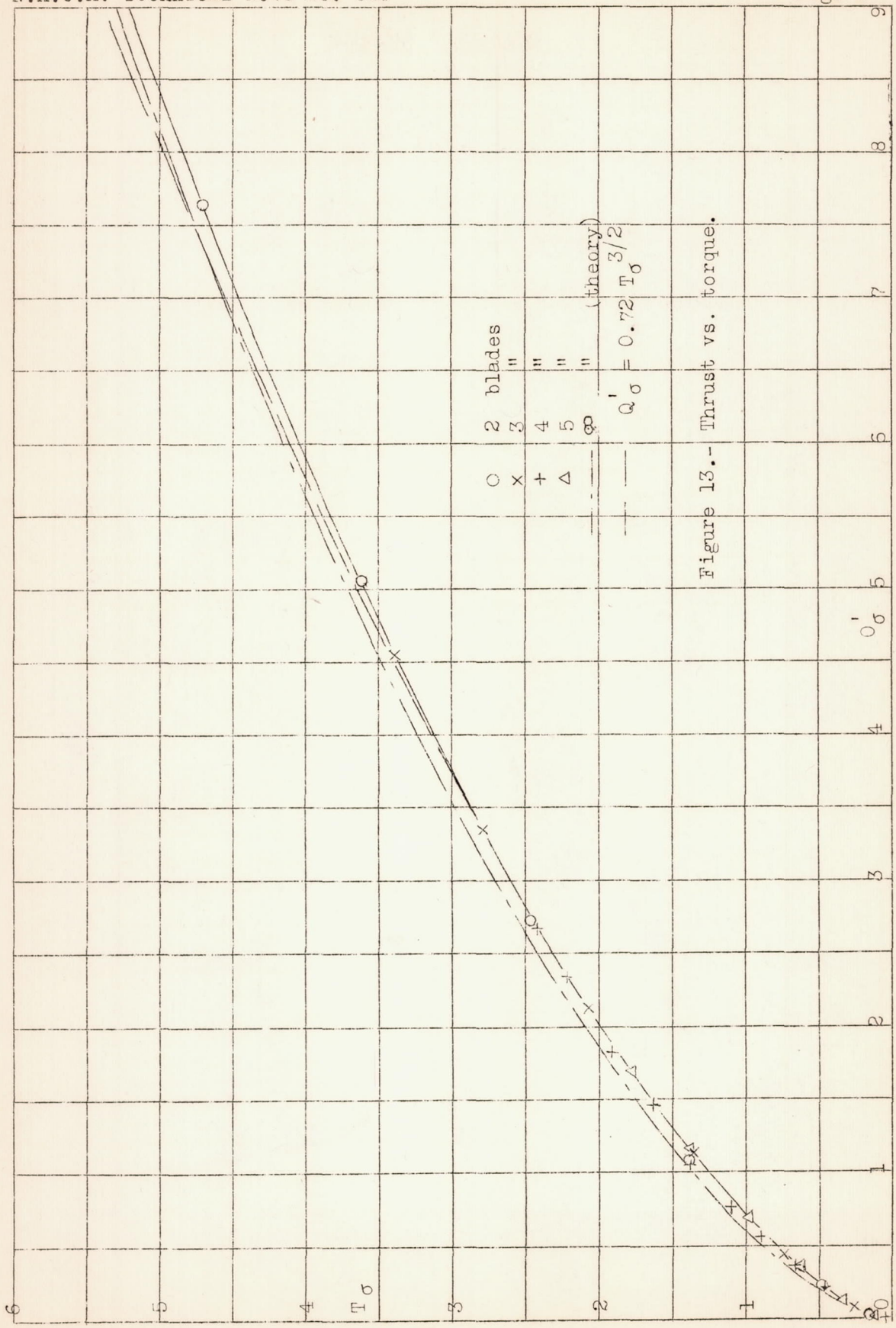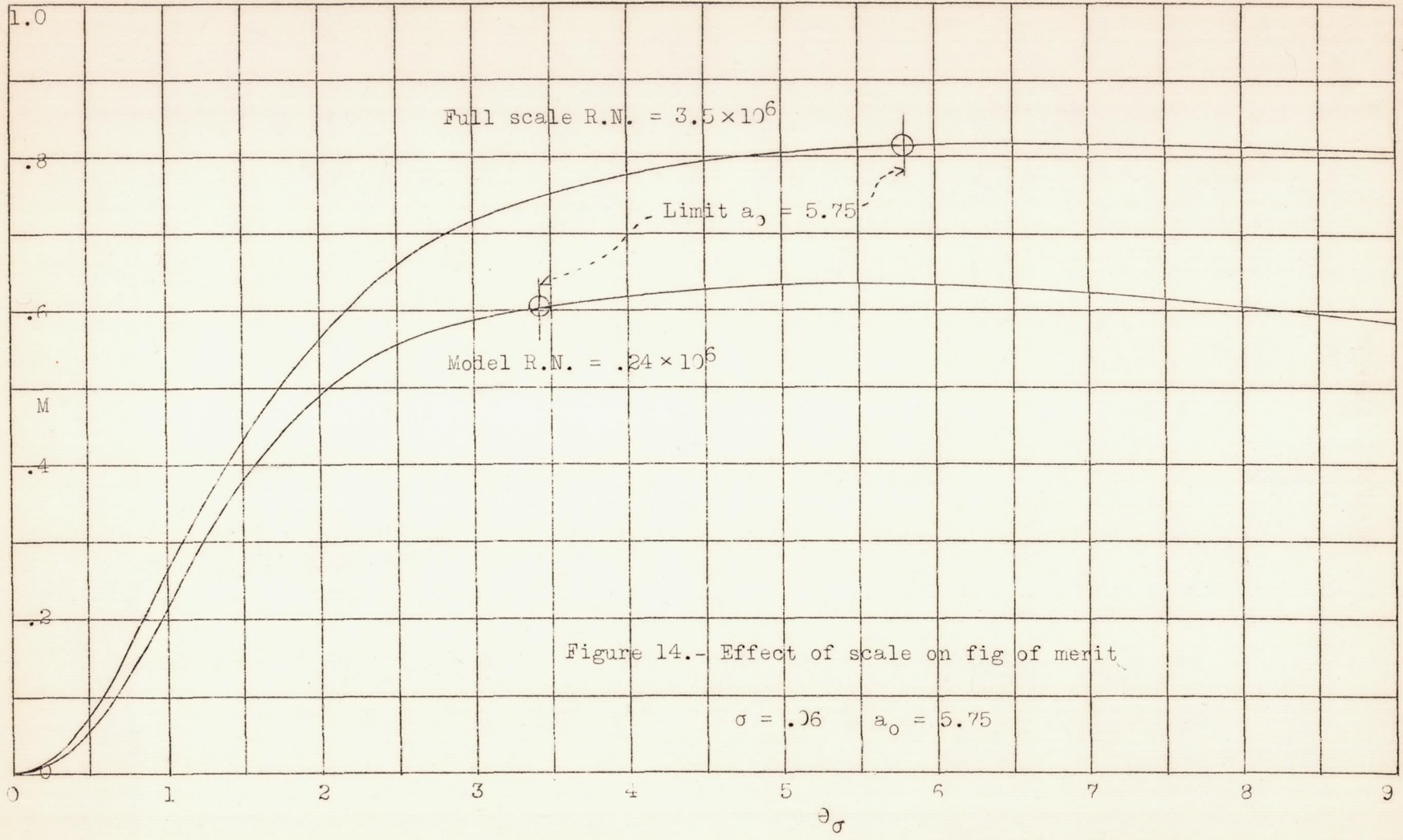
Figure 14.- Effect of scale on fig of merit

σ = .06 a_o = 5.75

Fig. 14

Figure 15.- Full scale thrust and torque coefficient. (Estimated)

$a_0 = 5.75$ $\epsilon = .30$

Fig. 15
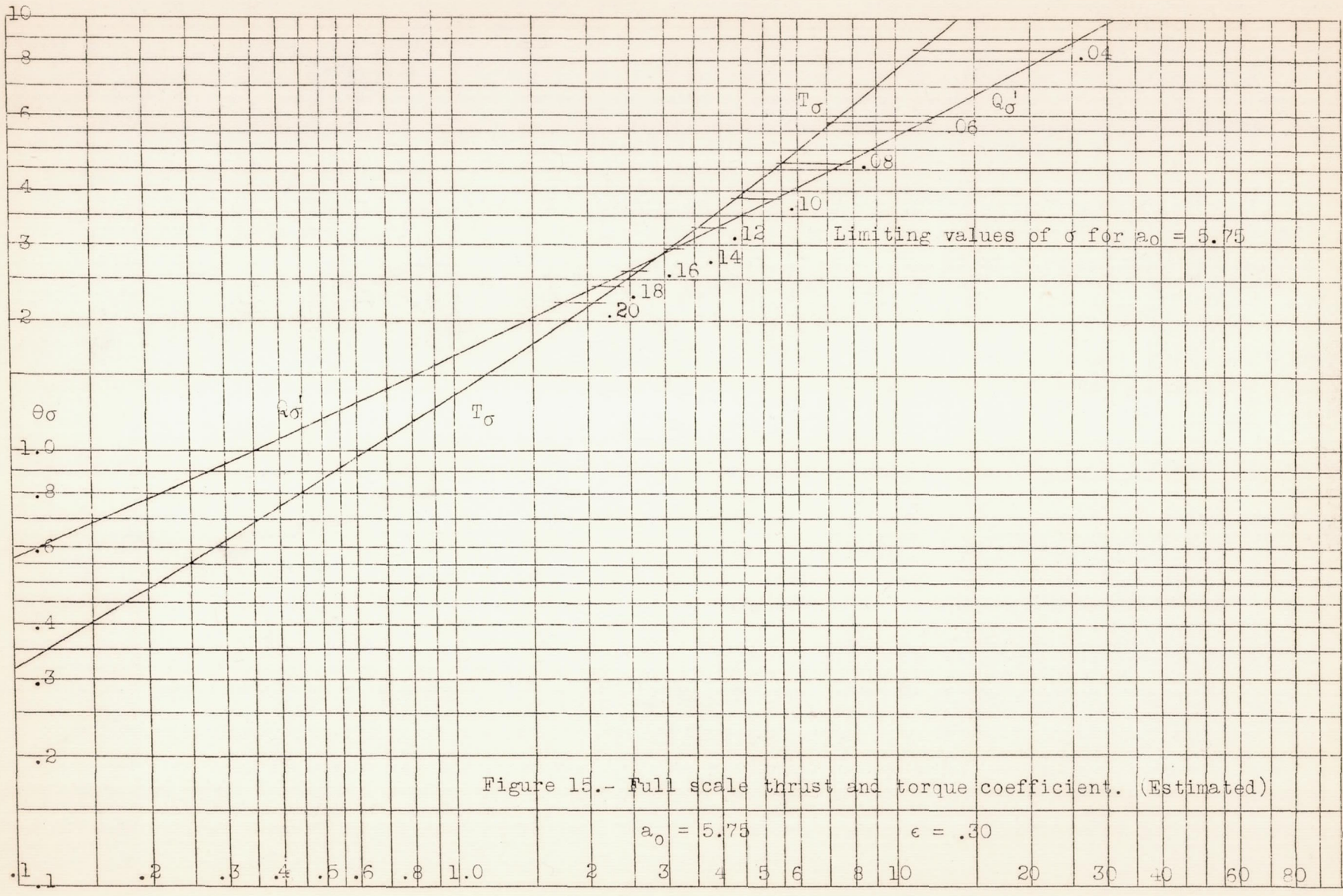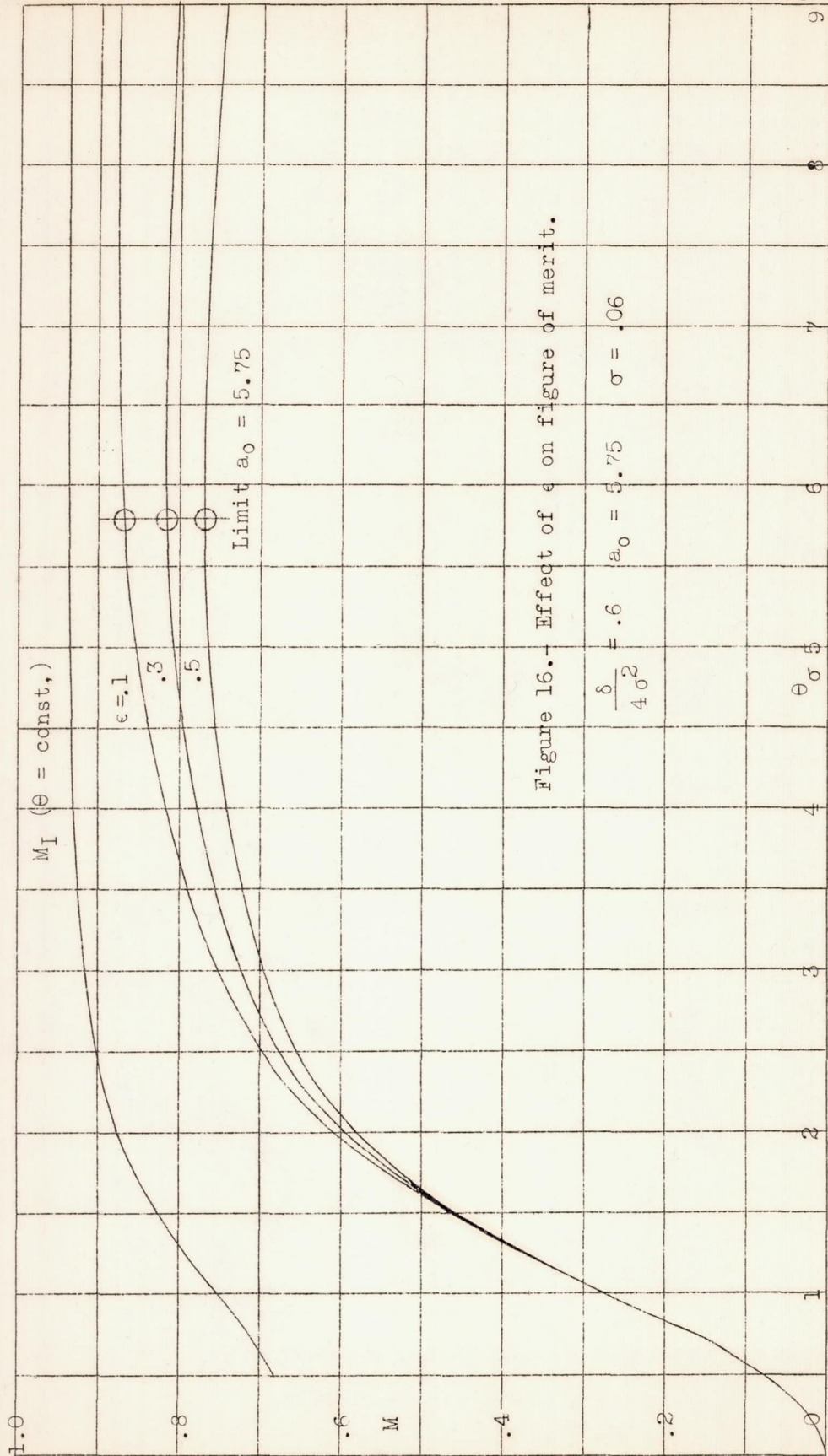
Figure 16.- Effect of ε on figure of merit.

$$\frac{\delta}{4\sigma^2} = .6 \qquad a_0 = 5.75 \qquad \sigma = .06$$
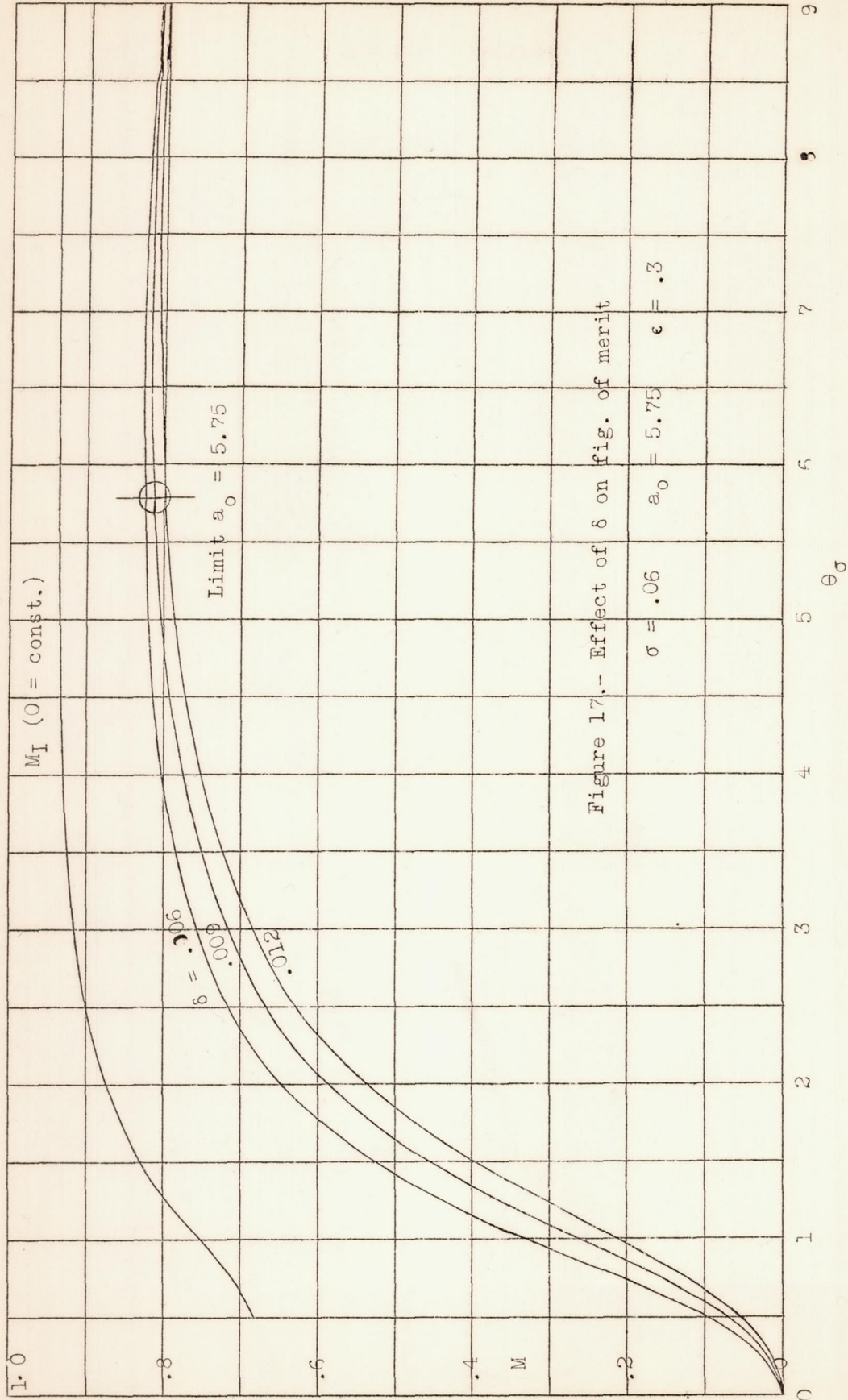
Figure 17.- Effect of δ on fig. of merit

$\sigma = .06$ $a_0 = 5.75$ $\epsilon = .3$

M_I (ρ = const.)

M_I (θ = const.)

M_I (modified theory)

ρ = const.

θ = const.

Limit a_0 = 5.75

Figure 18.- Effect of twist on figure of merit.

$$\frac{\delta}{4\sigma^2} = .6 \qquad a_0 = 5.75 \qquad \epsilon = .30 \qquad \sigma = .06$$

1.0

.8

.6

M

.4

.2

0

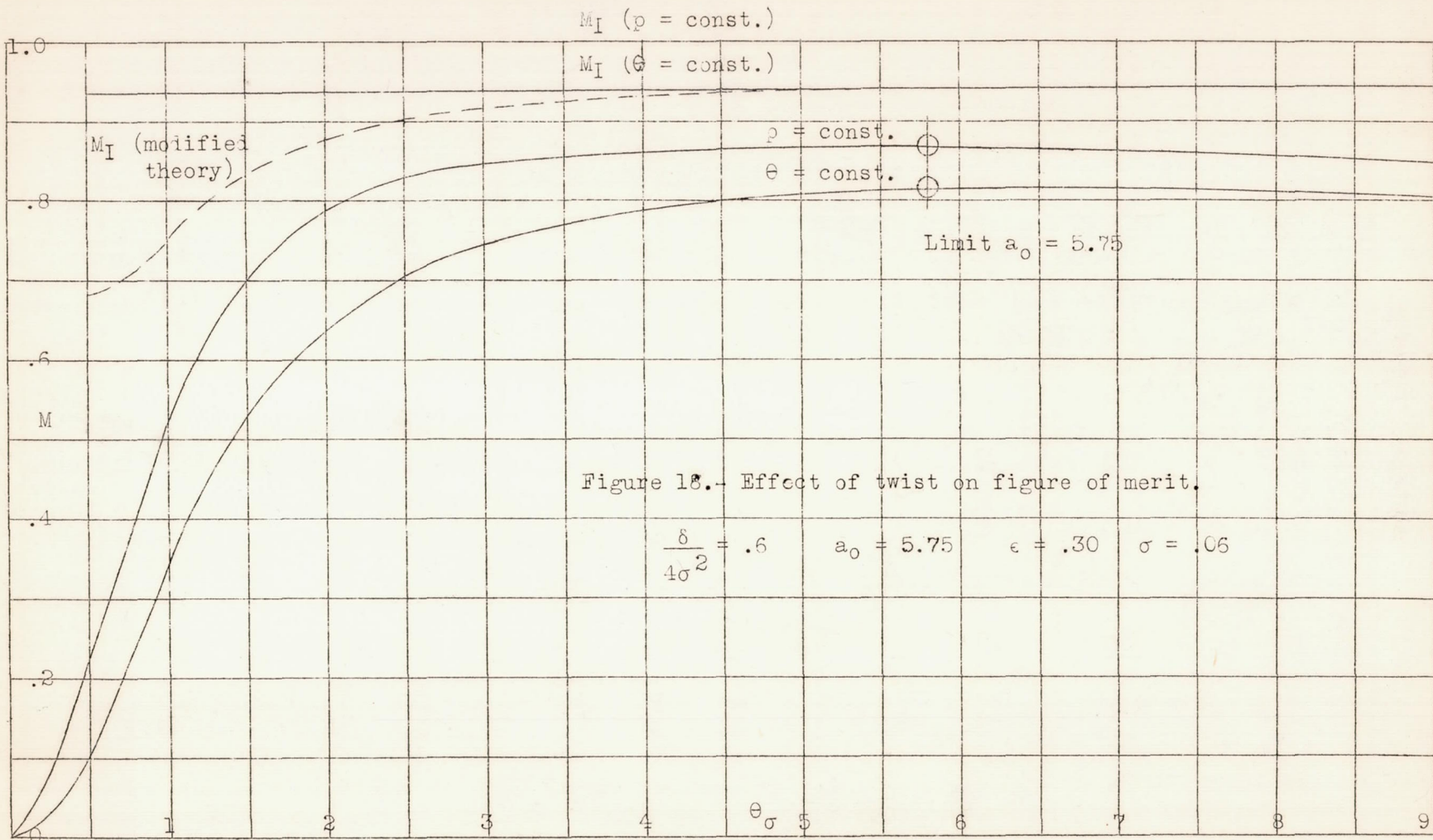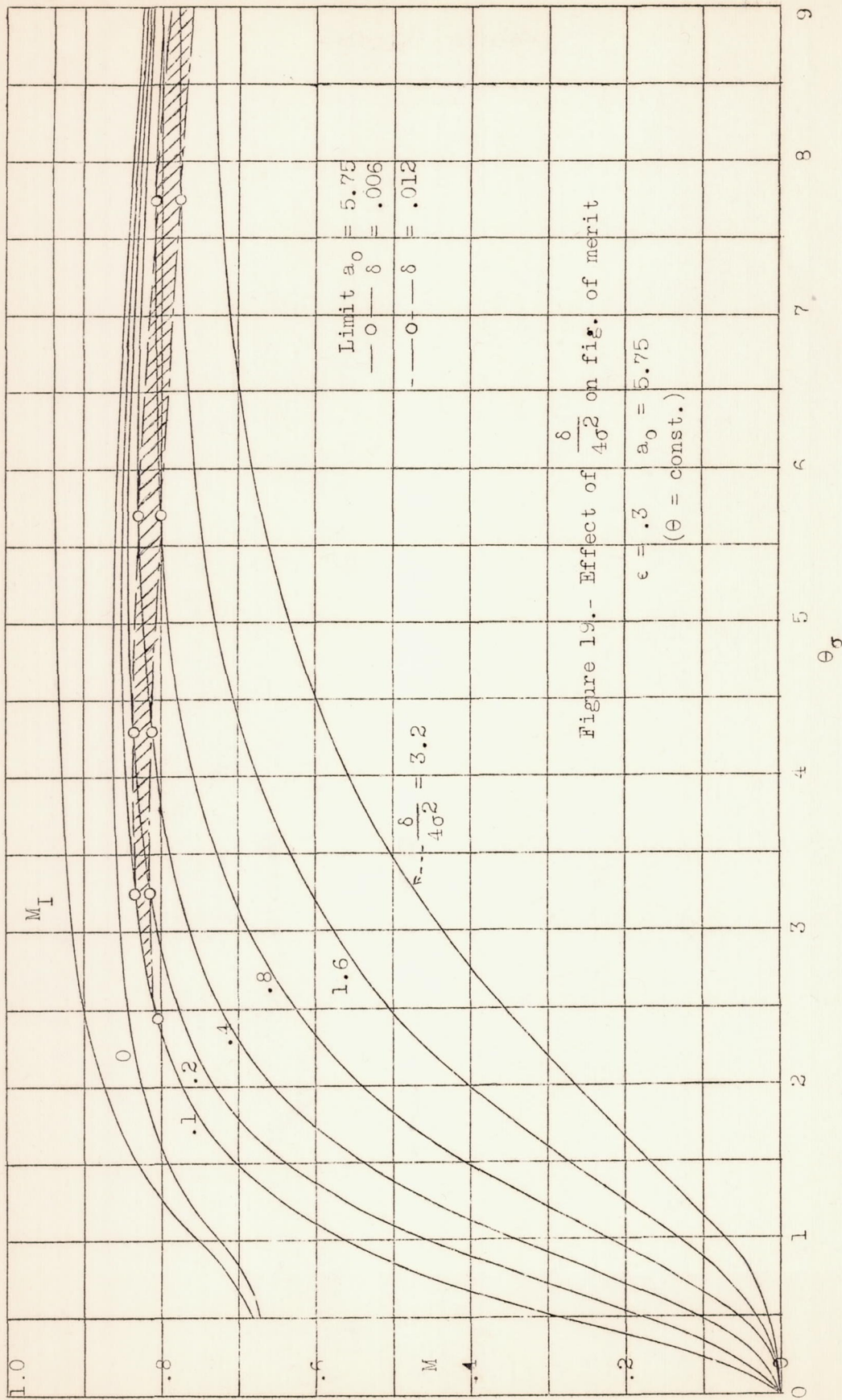0   1   2   3   4 θ_σ 5   6   7   8   9

Fig. 18

Figure 19.- Effect of $\dfrac{\delta}{4\sigma^2}$ on fig. of merit

$\epsilon = .3 \quad a_0 = 5.75$
$(\Theta = \text{const.})$

Figure 20.- Helicopter ceiling chart.
Hovering flight.

Fig. 21

Figure 21.- Helicopter loading chart.
Hovering flight.

$\frac{W}{MP'} = L_P$

$\frac{W}{\pi R^2} = L_s$